ГОСУДАРСТВЕННЫЙ НАУЧНЫЙ ЦЕНТР РОССИЙСКОЙ ФЕДЕРАЦИИ
ТРОИЦКИЙ ИНСТИТУТ ИННОВАЦИОННЫХ И ТЕРМОЯДЕРНЫХ ИССЛЕДОВАНИЙ

TROITSK INSTITUTE FOR INNOVATION AND FUSION RESEARCH

ÐÎÑÑÈÉÑÊÀß ÀÊÀÄÅÌÈß ÍÀÓÊ
RUSSIAN ACADEMY OF SCIENCES
P.N. LEBEDEV PHYSICS INSTITUTE

Физический институт имени П.Н.Лебедева
Ф И А Н

Experimental and Theoretical Search of Conditions for Maximum Efficiency and for Frequency Tunability of IR Overtone CO Laser

Phase I.

Scientific Report

Time period: July 1997 - March 1998

*The research work has been done in accordance with a special contract **SPC-97-4066** with European Office of Aerospace Research and Development*

Contract F61708-97-W0215

Principal Investigator, Scientific Leader, Prof. A. Ionin

Scientific Leader, Prof. A. Napartovich

Mr. A. Kotkov

Dr. A. Kurnosov

Mr. L. Seleznev

Mr. N. Turkin

Mr. D. Sinitsyn

Mr. Y. Klimachev

Mr. L. Afanas'ev

Moscow, 1998

TABLE OF CONTENTS

1. INTRODUCTION

The main objective of the scientific work was an experimental and theoretical search of conditions for maximal efficiency of the first overtone (FO) CO laser and a study of a feasibility of lasing band broadening. In (Ionin et al, 1997) a comprehensive study of FO CO laser with suppressed fundamental band (FB) lasing has been done. By using an intracavity spectral filter suppressing FB lasing, output efficiency of 3% and specific output energy of ~ 10 J/l·Amagat were obtained, lasing taking place from 13→11 up to 25→23 vibrational transitions (λ = 2.7-3.3 μm). Some recommendations were formulated. In particular, there were proposed a decrease of intracavity useless optical lasses.

In accordance with these proposals, an improved spectral filter for suppressing FB lasing was developed and used in the experiments. Parametric study of FO CO laser operating with the new filter was carried out both experimentally and theoretically. In addition to the new filter, a set of dielectric mirrors with various spectral characteristics were used as output couplers with a purpose of lasing band broadening and frequency tunability. Theoretical studies of the frequency tunability of the FO CO laser were also performed. An improved self-consistent theoretical model and a numerical code capable to predict stability limits for electric discharge was proposed.

2. PARAMETRIC STUDY OF FO CO LASER AIMED AT HIGHER OUTPUT EFFICIENCY AND LASING BAND BROADENING

The results of the experimental research of FO CO laser are presented in the Chapter. The main objective of the research was a study of a feasibility of obtaining higher output efficiency and specific output energy (SOE), and lasing band broadening as compared to results, which we published in the previous Report (Ionin et al, 1997). A comparison of the experimental data with theoretical results is accomplished.

2.1 Experimental setup and measuring system

The experimental research of FO CO laser was carried out on cryogenically cooled e-beam controlled discharge (EBCD) laser setup. Active length was 1.2 m, electrical discharge volume 18 *l*. Active optical volume can be varied between ~ 0.1 and 10 liters by using optical diaphragms. Electron beam current density was up to 10 - 20 mA/cm^2, electron energy being 150 keV. Averaged current density of electric discharge was ~ 1 A/cm^2. Detailed description of the laser facility and measuring system is presented in (Ionin et al, 1996).

A laser spectrum was detected by home-made spectrograph based on diffraction grating (150 lines/mm), with maximum reflectivity for a wavelength of 4.0 μm. IR camera was used for detection of the laser spectrum in focal plane of the spectrograph. One could see laser spectrum on the display. He-Ne laser was used for a calibration of the spectrograph. A measuring accuracy was 0.01 μm. Spectral line intensity was determined visually by comparing a brightness of given line on display's screen with a brightness of the most intensive spectral line. All the spectral lines were divided into the three groups: strong, medium and weak intensities. Sometimes, we divided lines in the given group by using the same way.

For measuring temporal characteristics, PEM photodetector given us by AFRL was used. For measuring spectral-temporal characteristics, it was situated in a focal plane of the spectrograph.

2.2. FO CO laser with new spectral filter

2.2.1 Development of new spectral filter

In (Ionin et al, 1997) we came to the conclusion for the output efficiency of FO CO laser with suppressed FB lasing to be able to be increased by reduction of the intracavity useless optical losses. To suppress FB lasing we used there, as a spectral filter (SpF1), the plane parallel plate made of fused silica with a thickness of 1.9 mm. The size of the filter was 100x100 mm^2. The optical losses, connected with absorption and scattering, were estimated to be ~ 1% mm^{-1} for wavelength region of 2.5 - 3.3 μm. The spectral filter SpF1 was opaque for the wavelengths of FB.

Following the conclusion of the previous Report, a new spectral filter (SpF2) with lower optical losses was researched and developed.

The preliminary estimation showed us, that to see a substantial improvement in laser characteristics due to diminished absorption, the thickness of the filter plate should be lowered 4-5 times. Hence, the estimated thickness should be about 0.4-0.5 mm. The diameter of the part of the filter plate illuminated by laser radiation should be at least 50 mm. Even at this aperture, taking into account that the plate is declined in the cavity at the Brewster angle of 54°, the diffraction losses in the cavity became essential. It means, that the ratio of the filter plate thickness to the diameter should be lower than 0.01. From the other hand, the surface roughness, when measured by an interferometer in the transmission configuration, should not exceed one fringe at the λ = 0.63 μm. Tolerances in respect to plane parallel geometry are not so stringent, the wedge with the angle θ = 1 mrad is acceptable. Nevertheless, the problem to manufacture this plate is a difficult one, and requires deliberate manual working, the result depending on skill and qualification of the master. We succeeded in manufacturing of the plate of this sort.

The diameter of this filter plate is 55 mm and the thickness 0.41 mm with the wedge θ = 0.4 mrad. With a help of the spectrophotometer "Perkin-Elmers G983", spectral dependencies for transmission and reflection coefficients of old and new spectral filters were measured. It allows us to find with a good accuracy the dispersion of the refractive index and absorption for both filters in the spectral range of 2.0 - 4.0 μm. As a result, cavity losses associated with absorption and reflection from the filter plate for every spectral line of the FO CO laser can be calculated for a given inclination angle of the filter plate relatively to the optical axis. Dependencies for the thick and thin spectral filters versus radiation wavelength are presented in **Fig.2.1**. The experimental results on a study of spectral characteristics of the two filters at different inclination angles are presented in **Appendix I**.

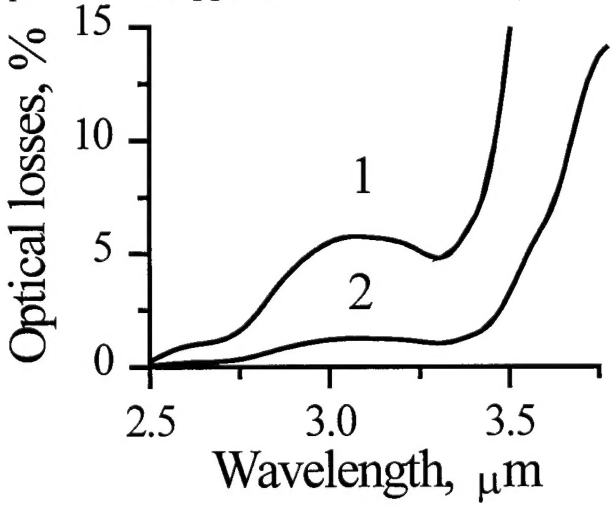

Fig.2.1. Measured spectral optical losses inside old thick (1) and new thin (2) spectral filters located under 33° to the optical axis.

2.2.2. Parametric study of FO CO laser with new spectral filter

The comparative spectral characteristics of the two spectral filters either thick or thin one and experimental spectra of the FO CO laser are presented in **Fig.2.2**. In fact, the spectral transmittance of the new filter (b) is much higher as compared to old ones (a) in long wavelength spectral band. As a result, the spectrum of the FO CO laser with SpF2 is broader. Lasing takes place in wavelength region of 2.7 - 3.6 μm (2.7 - 3.3 μm band in case of SpF1, **Fig.2.2**).

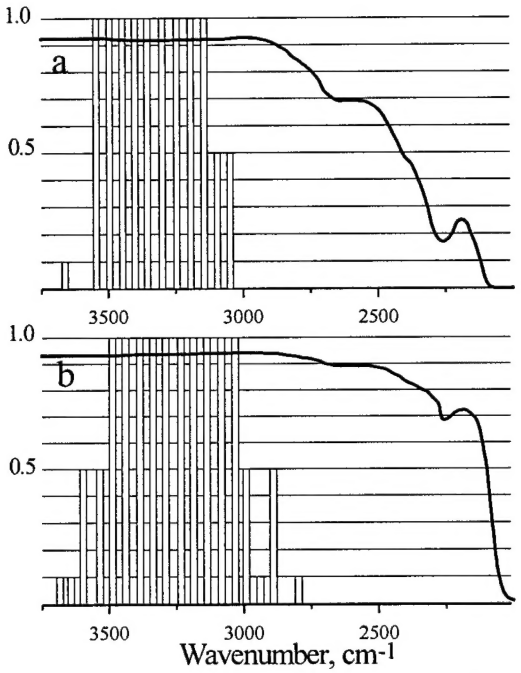

Fig.2.2. Spectral transmittances of the thick (a) and thin (b) spectral filters and corresponding spectra of the FO CO laser output.

Calculated and experimental FO CO laser spectra for the thin filter are presented in **Fig.2.3.** Comparing these spectra, the conclusion can be drawn about quite a good correlation between them. Irregularity of calculated spectra is explained by competition of two sets of radiating vibrational-vibrational transitions (cascades) in active medium of FO CO laser. These spectra were obtained in a frame of the homogeneous theoretical model. In the experiments such features of the spectra seem to be not observed because of the inhomogeneity of the real active medium and the visual method of estimation of the spectral lines intensities.

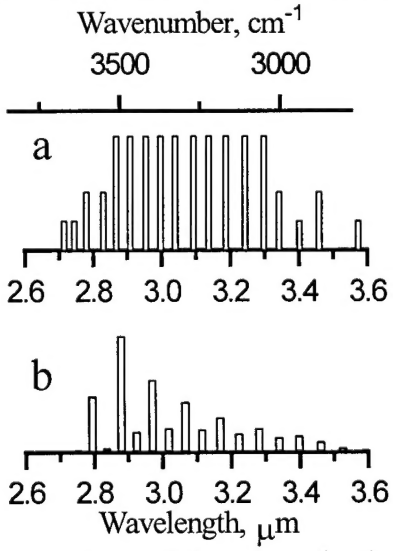

Fig.2.3. Experimental (a) and theoretical (b) spectra of the FO CO laser output for the thin spectral filter.

A comparison of the energetic characteristics of the FO CO laser using these spectral filters was carried out. The most effective (Ionin et al, 1997) gas mixture $CO:N_2:He = 1:9:10$ was used in the

experiment. The single-pass spectral transmittance of the new filter because of its less thickness was approximately 1 - 2% higher than that of old filter in the lasing range of FO CO laser. Therefore, using new spectral filter SpF2 enabled us to decrease the intracavity useless optical losses.

The dependencies of the laser efficiency on the SIE obtained for both filters are demonstrated in **Fig.2.4**. As a result, the decrease of the threshold SIE was observed from ~ 100 J/l Amagat for old filter down to 80 J/l Amagat for the new one. The behavior of the curve for SpF2 is practically the same as for SpF1 in the transmittance region of the both filters. However, one can see the output efficiency for the FO CO laser with SpF2 being approximately twice as much as that of the FO CO laser with the old filter. As SIE increased up from its threshold value, time delay between the beginning of pumping and laser pulses decreased down to 50-70 μs (**Fig.2.5**).

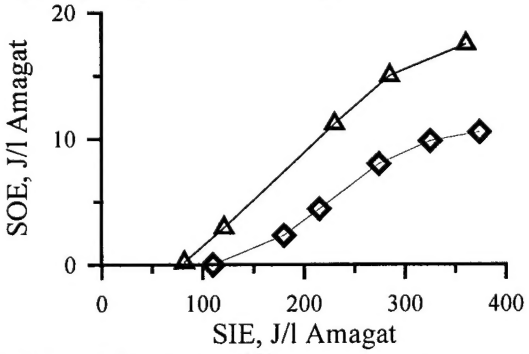

Fig.2.4. FO CO laser specific output energy versus specific input energy for laser resonator with the thick (a) and thin (b) spectral filters
CO : N_2 : He = 1 : 9 : 10; N = 0.3 Amagat

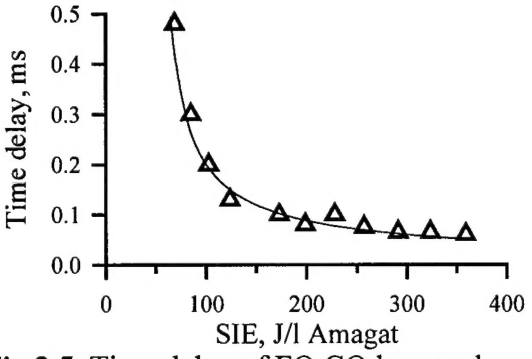

Fig.2.5. Time delay of FO CO laser pulse vs. specific input energy
CO : N_2 : He = 1 : 9 : 10;
N = 0.3 Amagat; T = 100 K

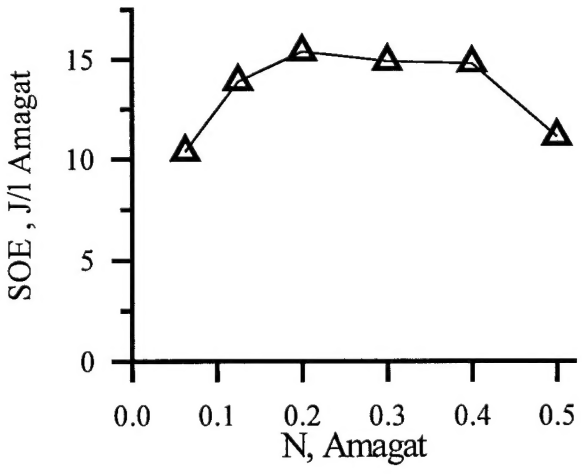

Fig.2.6. FO CO laser specific output energy vs. gas density
CO : N_2 : He = 1 : 9 : 10;
N = 0.3 Amagat; T = 100 K;
Q_{in} = 380 J/l Amagat

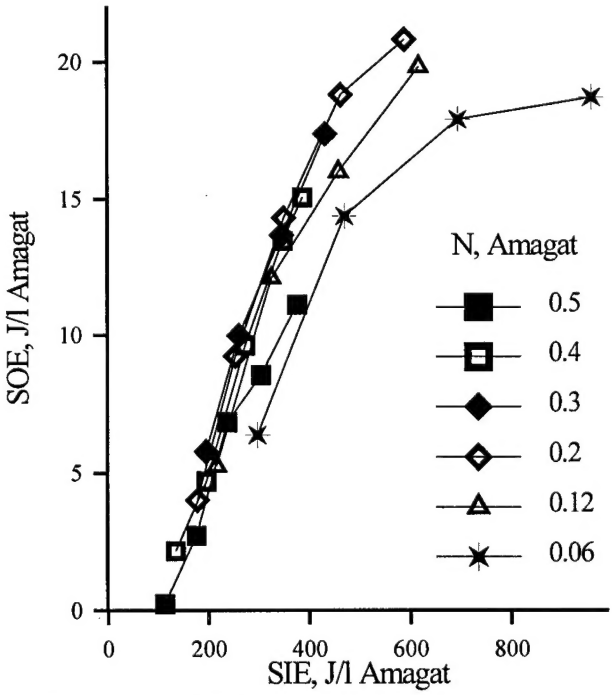

Fig.2.7. FO CO laser specific output energy vs. specific input energy for various gas density
CO : N_2 = 1 : 9; T = 100 K

Fig.2.6 demonstrates the dependence of the SOE on density of He-free gas mixture CO:N_2=1:9 at the same specific input energy of 380 J/l Amagat. Gas density varied within the range of

0.06-0.5 Amagat. Gas density variation within 0.2-0.4 Amagat had no effect on SOE and output efficiency, which came up to 15.4 J/l Amagat and 4%, respectively, being twice as high as those of FO CO laser operating on He-free gas mixture CO:N_2=1:9 with old thick filter. At higher SIE, specific output energy comes up to ~ 20 J/l Amagat.

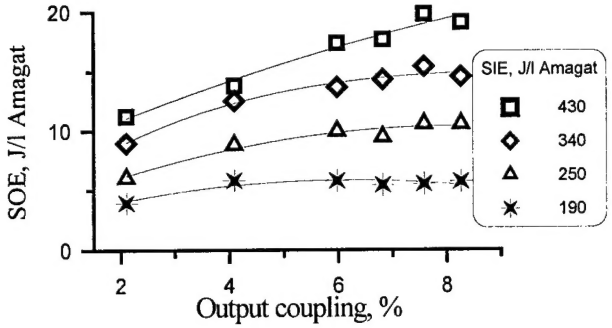

Fig.2.8. FO CO laser specific output energy vs. output coupling
CO : N_2 = 1 : 9; N = 0.3 Amagat;
T = 100 K; Q_{in} = 195 J/l Amagat

The usage of He containing gas mixtures also enabled us to increase the SOE up to ~20 J/l Amagat (approximately, at the same SIE as in **Fig.2.6**), that one can see from **Fig.2.8** representing the SOE versus output coupling for various SIE. The output coupling was controlled by angular inclination of the new spectral filter relatively to optical axis. For instance, the angle of 27° corresponded to the effective output coupling of ~7% (detailed information see in **Appendix I**).

A comparison of experimental dependence of SOE on gas temperature with theoretical one is presented in **Fig.2.9** for SIE of 200 J/l Amagat. Experimental data were obtained for SIE of 220, 280 and 350 J/l Amagat. The lasing threshold only was observed at gas temperature of 170 K. Gas mixture cooling from 165 K down to 114 K resulted in considerable increase of SOE (from 0.01 up to 15 J/l Amagat for SIE of 350 J/l Amagat). The general trend for the experimental and theoretical curves (SIE of 220 J/l Amagat) is in an adequate agreement, calculated SOE being of 4 J/l Amagat higher as compared to experimental one.

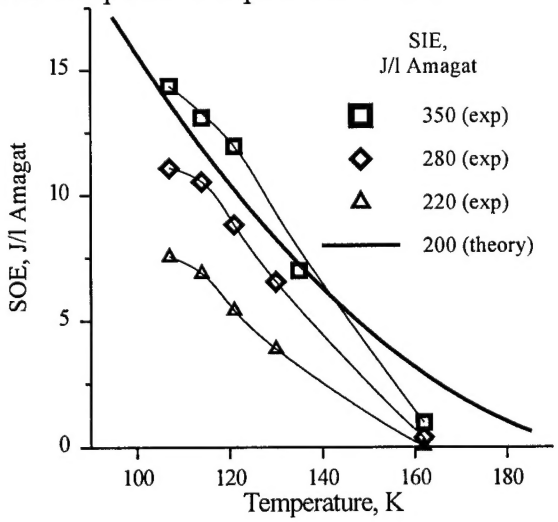

Fig.2.9. FO CO laser specific output energy vs. gas temperature for different specific input energy.
CO : N_2 : He = 1 : 9 : 10; N = 0.3 Amagat

Previous estimations demonstrated, that even little change of useless intracavity optical losses had a considerable effect on output efficiency and SOE of FO CO laser. That is why we researched an influence of intracavity diffraction losses on SIE (**Fig.2.10 - 2.13**) and also made an extrapolation to estimate the effect of useless optical losses on output efficiency (**Fig.2.14**). Intracavity diffraction losses changed by changing the diameter of intracavity diaphragm from 36 down to 7 mm, Fresnel number $N_F=a^2/\lambda L$ (where a is radius of aperture diaphragm, L is resonator length) being decreased from 43 down to 1.6 (λ = 3 μm). **Fig.2.10** demonstrates the dependence of SOE on N_F for different SIE (175, 230 and 290 J/l Amagat). For all the curves one can see a sharp rise of SOE versus N_F

within a range of 1.6-6.5, that can be explained by a decrease of diffraction losses at higher Fresnel numbers.

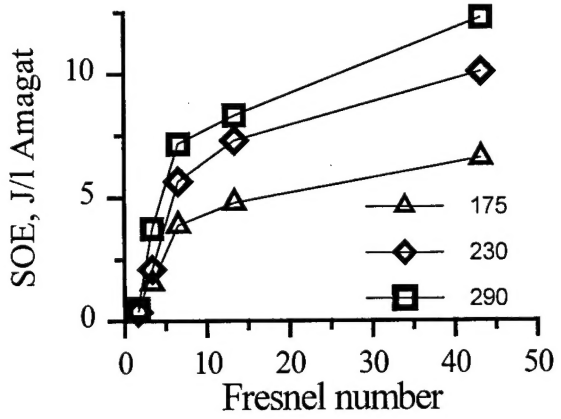

Fig.2.10. FO CO laser specific output energy vs. Fresnel number for different specific input energy
$CO : N_2 : He = 1 : 9 : 10$;
N = 0.3 Amagat; T = 100 K

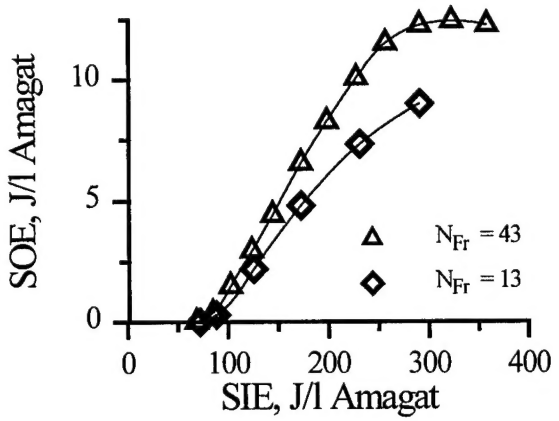

Fig.2.11. FO CO laser specific output energy vs. specific output energy for two Fresnel numbers
$CO : N_2 : He = 1 : 9 : 10$;
N = 0.3 Amagat; T = 100 K

Fig.2.11 demonstrates SOE versus SIE for two different Fresnel numbers, SOE being notably higher at higher N_F. Better conditions for overtone lasing with Fresnel number rise, one can also see from **Fig.2.12**, where time delay for overtone lasing decreases at Fresnel number rise.

The new filter size did not allow us to increase the Fresnel number more than 50. The larger old filter gave us such an opportunity. **Fig.2.13** demonstrates the same dependency, as in **Fig.2.10** for thick filter, at various SIE of 160, 220 and 280 J/l Amagat. As the Fresnel number increases up to 30, one can observe SOE rise connecting with a reduction of diffraction losses. However, at N_F>30 there is a decrease of SOE, that can be due to thermal nonhomogeneity of FO CO laser active medium.

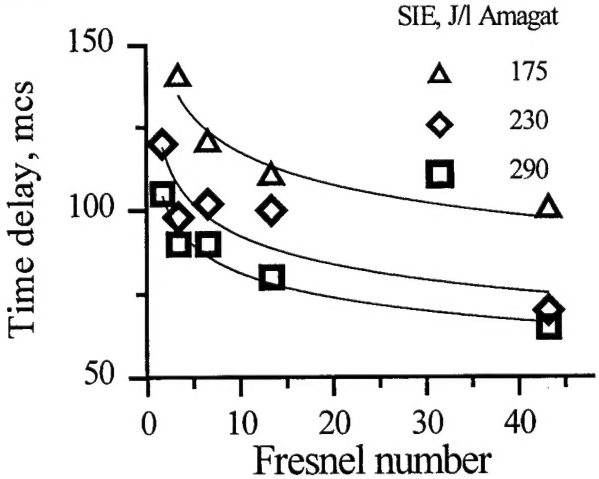

Fig.2.12. Time delay vs. Fresnel number for different specific input energy
$CO : N_2 : He = 1 : 9 : 10$;
N = 0.3 Amagat; T = 100 K

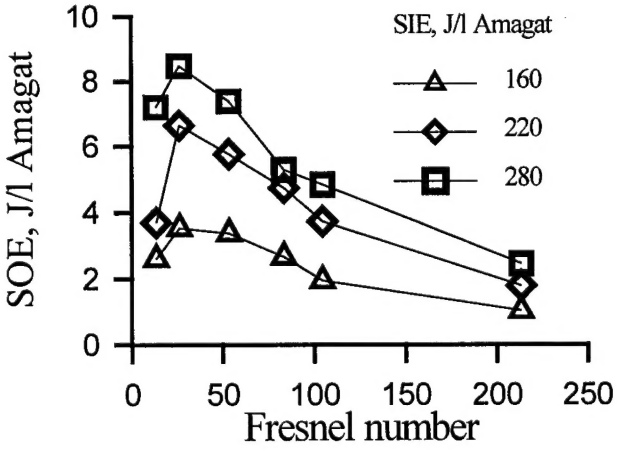

Fig.2.13. FO CO laser specific output energy vs. Fresnel number for thick filter
$CO : N_2 : He = 1 : 9 : 10$;
N = 0.3 Amagat; T = 100 K

Fig.2.14 summarizes experimental and theoretical results on the laser efficiency for the gas mixture $CO:N_2:He=1:9:10$ and demonstrates results of theoretical extrapolation, when useless

intracavity losses are diminished step by step. This can be achieved, for example, by increasing reflection coefficients of metal mirrors (or by substituting them by dielectric mirrors with higher reflectivity). The next step in diminishing useless optical losses can be realized by elimination of the losses in the output window. One can see, that the almost complete reduction of useless optical losses can result in the laser efficiency and SOE in the range of 15% and 50 J/l Amagat, respectively. It is possible also by changing the laser cavity construction to exclude the absorption of the laser radiation in atmosphere by water vapor. In this case the theory predicts the maximum laser efficiency and SOE as high as ~ 20% and ~ 80 J/l Amagat, respectively. **Fig.2.14** clearly demonstrates the possibilities of the FO CO laser in becoming effective laser source in the spectral region of 2.7-3.6 μm.

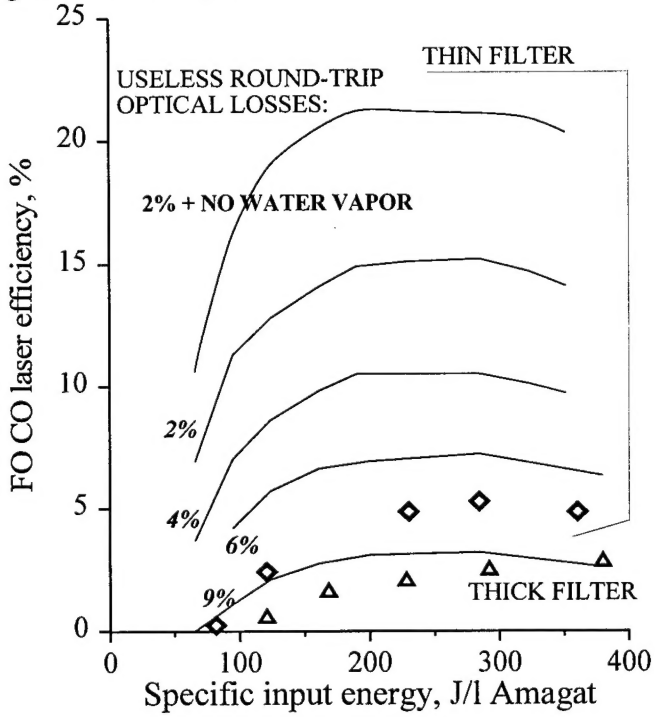

Fig.2.14. FO CO laser efficiency as a function of the SIE
$CO:N_2:He = 1:9:10$;
N = 0.3 Amagat;
T = 105 K, pumping pulse length 25 μs
◇△ experiment for the thin and thick filter, respectively

2.3 FO CO laser with dielectric mirrors

The Brewster window and atmospheric water vapor introduce additional optical losses to the FO CO laser cavity. The best solution of the problem would be using of dielectric mirrors with high reflectivity in the wavelength of 2.5-4.0 μm and very low reflectivity in the fundamental band, installed directly on laser chamber. So, in parallel with an order, which AFRL launched in the US, we also ordered two sets of mirrors in Russian company.

All the mirrors had a radius of curvature of 10 m, mirrors diameter being 70 mm. At first, mirrors from the first set (M1) are supposed to be output couplers for a symmetric FO CO laser resonator with on optimal effective coupling of 6-8% at the wavelength range of 2.5-4.0 μm (Ionin et al, 1997). Dielectric mirror from the second set (M2) had to be used as totally reflecting one for overtone spectral band and had to be used in combination with mirror M1. Special attention was paid to a reduction of mirror reflectivity for FB at wavelength longer than 4.8 μm. In particular, for the reflectivity reduction from the opposite mirror side, its surface had an antireflection coating with reflectivity less than 1% in the CO first overtone and fundamental bands. To prevent from coupling with back sides of the mirrors, their CaF_2 substrates had a wedge of ~ 15 mrad. Besides, the mirrors had to have optical threshold damage not less than 1-2 J/cm^2 and low absorption and scattering (< 1% at least). However, for producing a mirror with such a spectral characteristic, a large number of interference layers had to be in the mirror dielectric coating (19 layers in the our case), that

caused useless optical losses connected with absorption and scattering. The spectral characteristics of the mirrors manufactured for us are presented in **Appendix II**.

Our requirements to the above company were not entirely fulfilled. Reflectivity and transmittance for both of mirrors had a nonmonotonous behavior either in first overtone band or in fundamental band. Reflectivity in fundamental band being notably higher than 1% (**Fig.2.15**; see also **Appendix II**). There was not totally reflection for mirror M2 in overtone band. Despite these facts, we obtained rather positive results both for FO CO laser spectrum and laser efficiency, when using three various combination of the mirrors (M1+M1; M1+M2 and M2+M2).

Bearing in mind, that the best output efficiency was obtained for gas density of 0.1-0.2 Amagat (Ionin et al, 1997), and the higher gas density, the higher laser energy density on the mirror surface, i.e. the higher a feasibility of the mirror destroying, all the experiments were carried out with gas density of 0.12 Amagat. Laser mixture $CO:N_2:He = 1:9:10$ was used. Laser beam diameter was determined by intracavity diaphragms 50 mm in diameter situated not far from the mirrors.

FO CO laser spectra for lasers using three combinations of above mirrors (M1+M1; M1+M2 and M2+M2) at SIE of 300 J/l Amagat are presented in **Fig. 2.15a**. Effective reflectivities for an equivalent output mirror, defined as $(R_i R_j)^{0.5}$ ($i = 1, 2; j = 1, 2$) for the three combinations are also presented at the same figure.

As can be seen from **Fig. 2.15a**, we were able to suppress FB lasing only for one combination of the mirrors M2+M2, corresponding to the minimal reflectivity in FB.

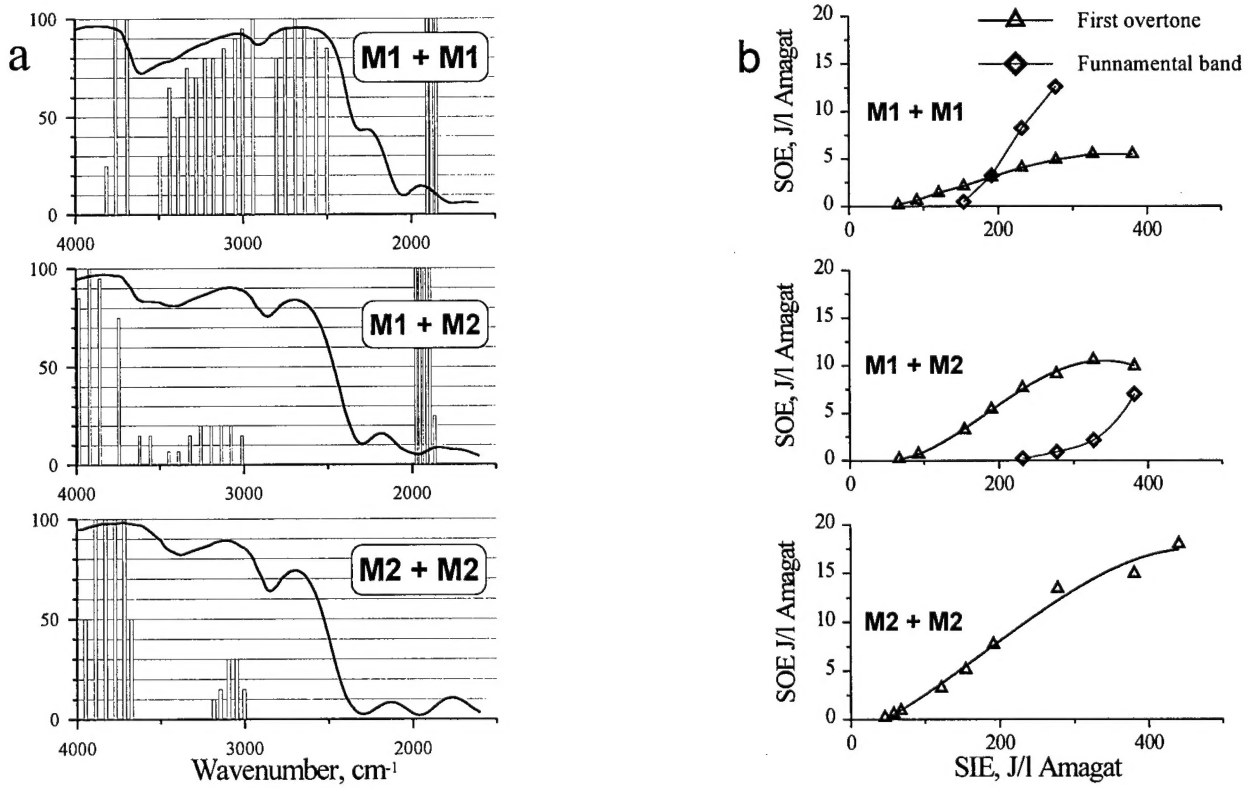

Fig.2.15. Laser output spectra (a) (first overtone and fundamental band) for three different output couplings (combinations of mirrors M1 and M2), effective reflectivities of the output mirrors and dependencies (b) of specific output energy on specific input energy
$CO : N_2 : He = 1 : 9 : 10$; N = 0.12 Amagat; T = 100 K

An analysis of FO CO laser spectra presented in **Fig. 2.15a** clearly demonstrate them to be strongly dependent on spectral properties of laser mirrors. Despite FB lasing for the mirror combination of M1+M1 and M1+M2, we observed FO lasing up to ~4.0 μm (M1+M1) and down to ~2.5 μm (M1+M2). In case of M1+M1 combination, FO CO laser spectrum consists of 20 vibrational bands from 9→7 up to 35→33 with wavelengths from 2.65 up to 3.95 μm. One can see quite a good correlation between the laser spectrum and reflectivity of the mirror. In case of M1+M2 combination the short wavelength border of the spectrum of 2.51 μm corresponds to vibrational transition 6→4. One can see from **Fig. 2.15a**, that relatively low reflectivity for some spectral region led to FO CO lasing suppression in the region, for instance, of 3.3-4.0 μm for M1+M2 combination, in the region of 2.71-2.86 μm for M1+M1 combination and in the region of 2.72-3.14 μm for M2+M2 combination. Therefore, pulsed FO CO laser can operate in the spectral region from 2.5 μm up to 4 μm, its spectral content being controlled by special characteristics of output coupler. It should be pointed out, that application of the dielectric mirrors considerably broadened the lasing spectral band as compared to previous Report (Ionin at al, 1997)

Energetic characteristics of FO CO laser with the dielectric mirrors are presented in **Fig. 2.15b** together with characteristics of FB CO lasing. Suppression of FB lasing resulted in considerable rise of maximum SOE from 5 J/l Amagat (M1+M1) up to 17 J/l Amagat (M2+M2).

FO CO laser spectrum strongly depends on SIE (**Fig.2.16**). In case of M1+M1 combination lasing starts for longer wavelengths. At higher SIE laser spectrum is broadened mostly to shorter wavelength region. (FB lasing started at SIE of 140 J/l·Amagat). The behavior observed can be connected with higher small signal gain for very high vibrational transitions of CO molecule.

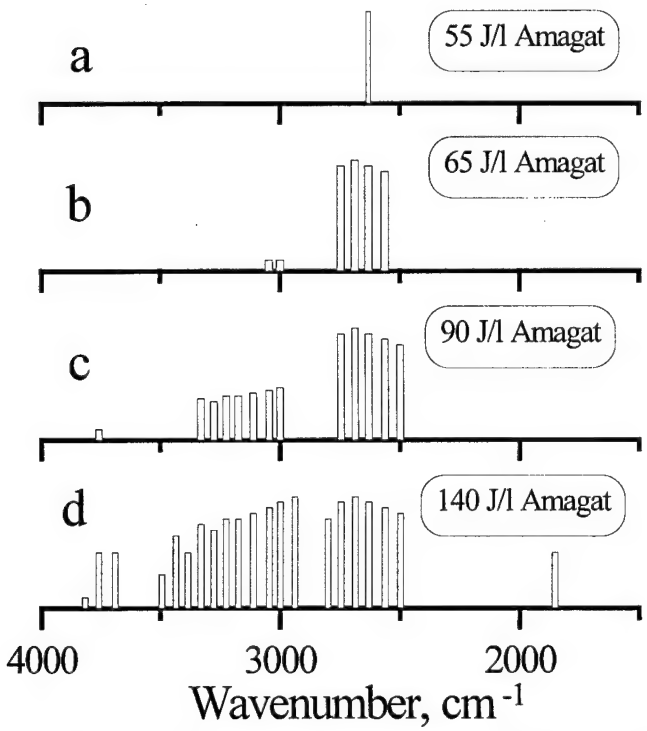

Fig.2.16. Alteration of FO CO laser spectrum for mirror combination of M1 + M1 with SIE rise

Temporal behavior of CO laser radiation (M1+M1) for various part of the laser spectrum (2.8 μm (a); 3.2 μm (b); 3.7 μm (c) and 5.3 μm (d)) is presented in **Fig.2.17** for SIE of 200 J/l Amagat. It should be pointed out, that for FO CO lasing, the longer wavelength, the longer laser pulse length and time delay between the beginnings of the laser and pumping pulses.

The FO CO laser spectrum calculated for M2+M2 combination is presented in **Fig.2.18**. One can see rather a good agreement between experimental (**Fig.2.15a**) and theoretical results.

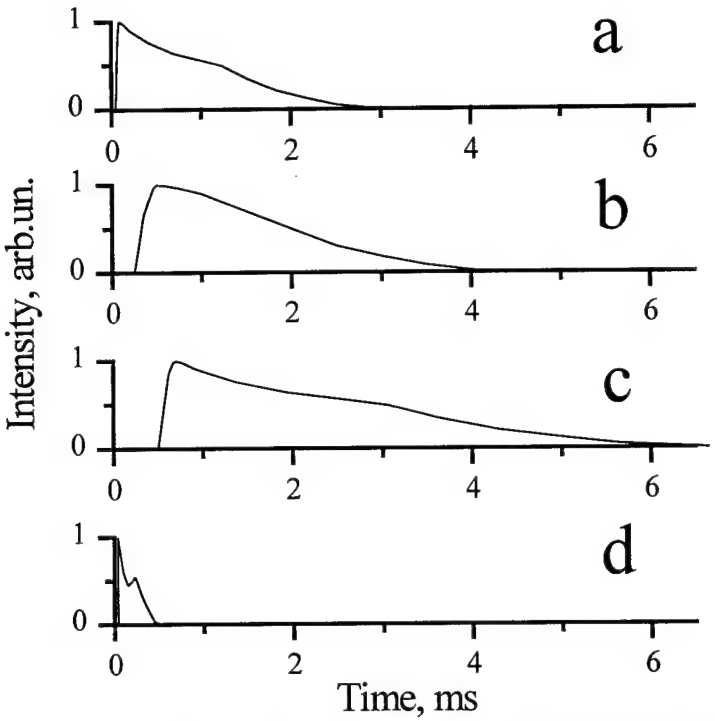

Fig.2.17. Time behavior of CO laser radiation for various parts of the laser spectrum:
2.8 μm (**a**);
3.2 μm (**b**);
3.7 μm (**c**);
5.3 μm (**d**).
Time delay is 90 μs (**a**); 250 μs (**b**); 500 μs (**c**) and 40 μs (**d**).
SIE = 200 J/l Amagat.

A comparison of experimental and theoretical data was accomplished also for energetic characteristics of FO CO laser with suppressed FB lasing (mirror combination M2+M2). **Fig.2.19** demonstrates the dependencies of output efficiency on SIE for various laser resonators (mirror combinations). The maximum efficiency of 5% was obtained for FO CO laser with suppressed FB lasing. It should be pointed out, that dielectric mirrors introduced rather high optical losses to the laser resonator, that was due to relatively high absorption and scattering (compare reflectivity and transmittance of the mirrors in **Appendix II**). Taking into account the optical losses, a calculation of laser efficiency was made. One can see in **Fig.2.19** quite a good agreement between the experimental and theoretical curves.

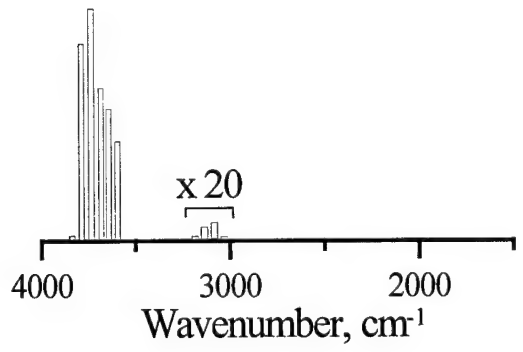

Fig.2.18. Theoretical output spectra obtained in calculations taking into account experimental conditions: optical resonator with mirrors M2+M2;
Q_{in} = 220 J/l Amagat.

Bearing in mind, that application of higher capacitance of capacitor bank lead to the better approximation of discharge voltage pulse by rectangular profile, i.e. to the low alteration of parameter E/N in the course of electric discharge, we compared energetic characteristics of FO CO laser for various capacitance from 33 up to 200 μF(**Fig.2.20**). Parameter E/N changed from 6 down to 1.5 kV/cm·Amagat for 33 μF and from 2.4 down to 2.0 kV/cm·Amagat for 200 μF, SIE being unchanged. Quite a different alteration of the parameter E/N could result in different efficiency of vibrational levels pumping in electric discharge and in different laser efficiency. However, we did not observe the difference for various capacitance (**Fig.2.20**).

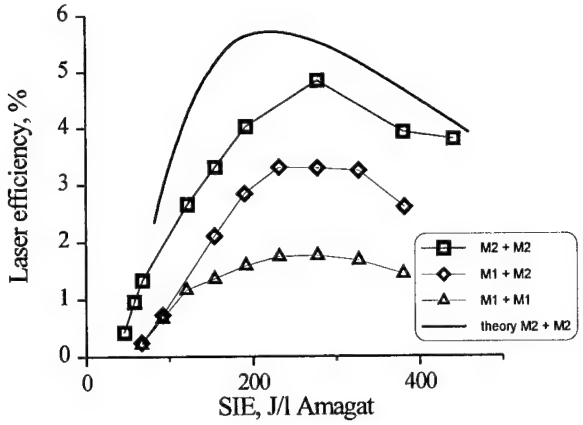

Fig.2.19. Experimental and theoretical efficiency of FO CO laser vs. specific input energy for different output coupling
$CO : N_2 : He = 1 : 9 : 10$;
N = 0.12 Amagat; T = 100 K

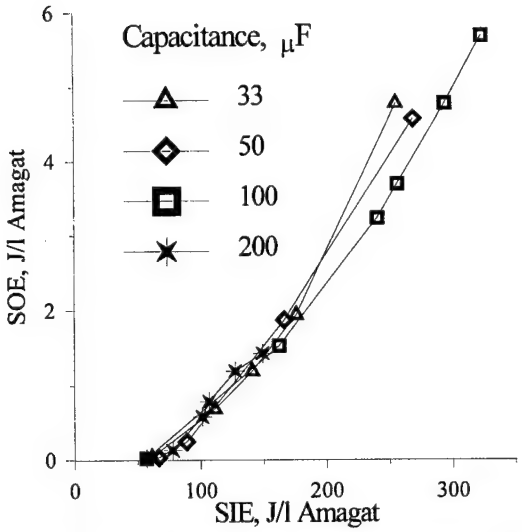

Fig.2.20. Specific output energy vs. specific input energy for different capacity banks
M1 + M1;
$CO : N_2 : He = 1 : 9 : 10$;
N = 0.12 Amagat; T = 100 K

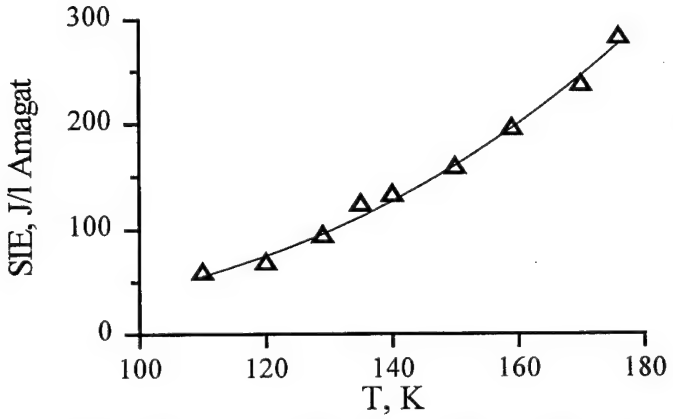

Fig.2.21. Threshold specific input energy vs gas temperature
M1 + M1;
$CO : N_2 : He = 1 : 9 : 10$;
N = 0.12 Amagat

Gas temperature has a very strong effect on FO CO laser energetic characteristics, in particular on threshold SIE (**Fig.2.21**), which increases from ~ 50 J/l·Amagat for ~110 K up to ~ 300 J/l·Amagat for 180 K.

Therefore, despite the special measures on reducing Q-factor of CO laser resonator for fundamental band, we could suppress FB lasing entirely only by using the mirror combination M2+M2 having the highest transmittance for wavelength longer than 5 μm. However, the resonator was far from optimal one needed for obtaining the highest FO CO laser efficiency, because of mirrors optical losses and, perhaps, because of narrow spectrum, limited by spectral characteristic of mirrors reflectivity (**Fig.2.15**). Nevertheless, the experimental results are in a good agreement with the theoretical data.

Besides, the experiments demonstrated a very important result, namely, a feasibility of pulsed FO CO lasing in a very wide spectral interval from 2.5 up to 4.0 μm on vibrational transitions from 6→4 up to 35→33. Application of various mirrors (and their combinations) demonstrated also, that FO CO laser spectrum can be tuned over the above spectral interval by means of dielectric mirrors (with high reflectivity for given part of FO CO laser spectrum).

3. CALCULATION OF FO CO LASER CHARACTERISTICS FOR FREQUENCY SELECTIVE CAVITY

As was demonstrated in previous Chapter, FO CO lasing proceeds simultaneously on many vibrational transitions covering the spectral range from 2.5 up to 4.0 μm. If somebody needs to have single-frequency radiation or radiation with controlled spectrum, this can be realized in two ways: by virtue of application of an external selection of the multifrequency laser output or by using a selective cavity. The second way looks more advantageous, because the laser pulse energy at the fixed transition can be increased. It is possible also to lase on transitions absent in the free-running laser spectrum. Some idea of how many discrete frequencies may be realized in the laser spectrum is given by the **Table AIII** in **Appendix III**, where the frequency and wavenumber values are presented for more than 800 rotational-vibrational transitions in overtone spectrum (P-branch) of $^{12}C^{16}O$, $^{13}C^{16}O$ and $^{12}C^{18}O$ molecules. The used spectroscopic data were taken from (Guelachvili et al, 1983).

Here we compare both methods of production of the single-frequency radiation putting an emphasis on studies of selective cavity lasing.

For calculations of a laser energy at a selected radiation transition the previously formulated model (Ionin et al, 1997) was used. At the selected vibrational level number, the rotational quantum number was defined as one having the maximum gain. Calculations were made for the following conditions: CO: N_2: He = 1: 9: 10; N = 0.3 Amagat; T_0 = 105 K, discharge current pulse duration 20 μs; the specific energy input 190 J/l Amagat; $(E/N)_0 = 0.9\ 10^{-16}$ V/cm^2.

First, possibilities to operate in the single-frequency mode were studied for conditions, when a reflective diffraction grating was employed. It was assumed that the diffraction grating selecting the laser transition operates in autocollimation mode and has the fixed reflectance independent of frequency. Output radiation was coupled out with the same grating when reflecting at the zero order. The output coupling was taken as 6% being equal to that of used in earlier studied free-running lasing (Ionin et al, 1997). It was assumed that no special measures were undertaken to remove water vapor absorption in the cavity.

In calculations the number of the upper vibrational level was fixed, while the rotational number in P-branch was calculated in the code from the condition the gain being higher than the threshold. As a result, consecutive lasing on several (2 or 3) rotational transitions was observed. For comparison, calculations were made when the rotational number was fixed, too (one of 2 or 3 transitions mentioned above). In these calculations the laser efficiency for the single transition coincides with a high accuracy (1-5%) with the total efficiency in modeling allowing for a free rotational transition. Therefore, the results of calculations with fixed vibrational and rotational numbers, both, may serve as an upper limit for laser efficiency at the given upper vibrational level. The predicted numerically laser efficiency for the described above conditions and the grating reflectance R = 80% is shown in **Fig.3.1** as a function of the upper vibrational level number. One can see that CO overtone laser with line selection has the efficiency of the order of 0.1% in this case.

The possibilities to increase the single-line laser efficiency by increasing the grating reflectance were studied. The results are displayed in **Figs.3.2** and **3.3** for R = 85% and R = 90%, respectively. Comparing **Figs.3.1** and **3.3**, the laser efficiency for some transitions may increase due to the higher reflectance (90 vs. 80%) more than an order of magnitude. The effect is still stronger for transitions between high lying levels.

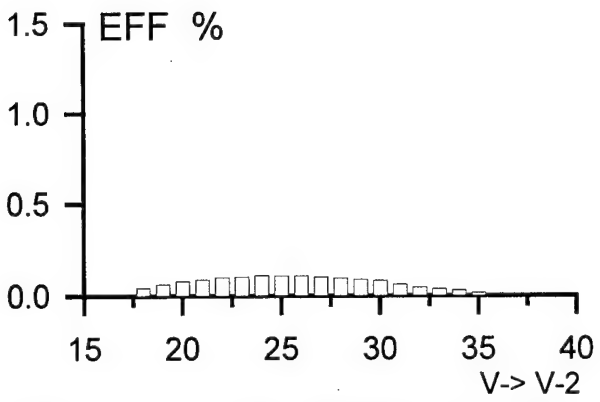

Fig. 3.1. FO CO laser efficiency versus the number of the laser upper vibrational level **v** for selective resonator. The grating reflectance in autocollimation mode R=80%.

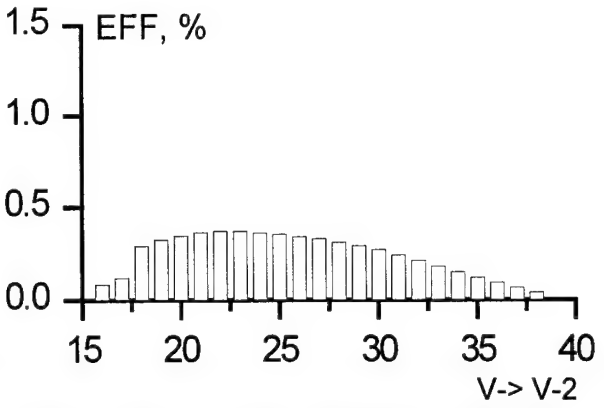

Fig. 3.2. FO CO laser efficiency versus the number of the laser upper vibrational level **v** for selective resonator. The grating reflectance in autocollimation mode R=85%.

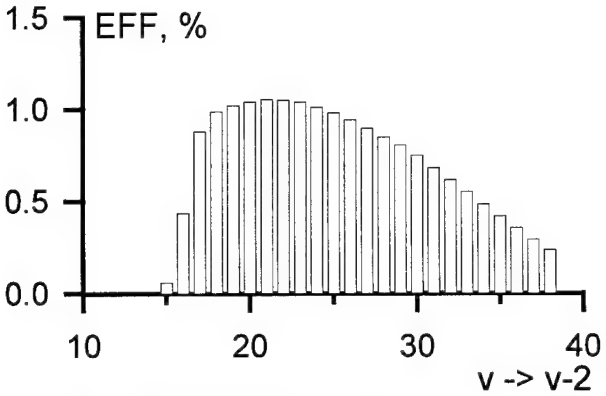

Fig. 3.3. FO CO laser efficiency versus the number of the laser upper vibrational level **v** for selective resonator. The grating reflectance in autocollimation mode R=90%.

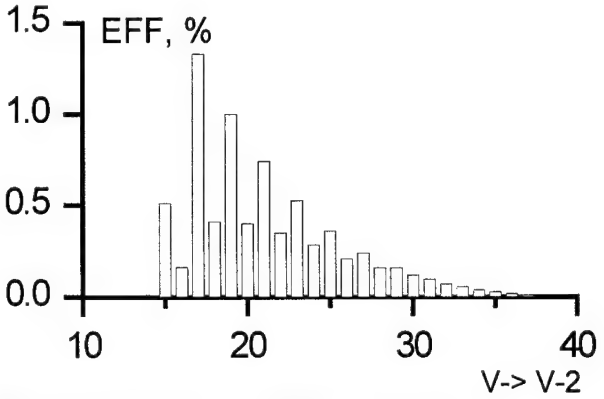

Fig. 3.4. FO CO laser efficiency for a separate transition (**v** is the number of the laser upper level) calculated for a free-running mode. The threshold conditions for all laser transitions correspond to Fig.3.3.

It is of interest to compare laser efficiency as a function of the upper laser level number for two situations: 1. Tuned selective cavity and 2. Free-running mode in the cavity without frequency selection. In both cases the threshold gain was supposed to be the same and its dependence on the radiation frequency is associated only with water vapor absorption. Approximately this threshold gain for $v > 17$ may be replaced by a constant $6.4\ 10^{-3}$ cm^{-1} because the water vapor absorption for these transitions is negligible.

The free-running frequency-integral laser efficiency was computed to be 7.3%. The respective laser efficiency for a separate transition as a function of its number is shown in **Fig.3.4**. Comparing **Figs.3.3** and **3.4** it is seen that using of selective cavity allows one to have a remarkable increase in spectral brightness of the laser radiation for vibrational transitions higher than 19→17. In the range of lower transitions where the spectral laser efficiency for the free-running mode has a maximum, application of the selective cavity does not allow to get the increase in laser efficiency and may even lead to some diminishing of it.

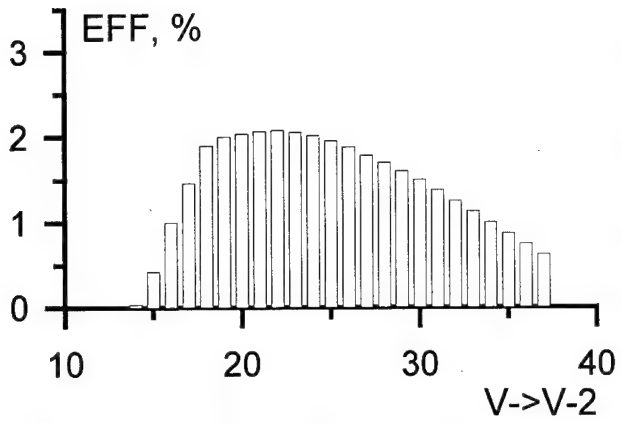

Fig. 3.5. FO CO laser efficiency for the selective cavity providing lasing on three neighboring vibrational transitions: $\mathbf{v_c - 1 \rightarrow v_c - 3}$, $\mathbf{v_c \rightarrow v_c - 2}$, $\mathbf{v_c + 1 \rightarrow v_c - 1}$ ($\mathbf{v_c}$ is the upper level number for the central transition). The threshold conditions for all laser transitions correspond to **Fig.3.3**.

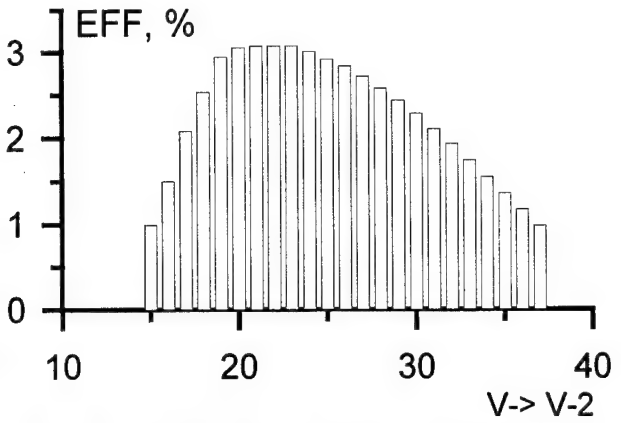

Fig. 3.6. FO CO laser efficiency for the selective cavity providing lasing on five neighboring vibrational transitions: $\mathbf{v_c - 2 \rightarrow v_c - 4}$, $\mathbf{v_c - 1 \rightarrow v_c - 3}$, $\mathbf{v_c \rightarrow v_c - 2}$, $\mathbf{v_c + 1 \rightarrow v_c - 1}$, $\mathbf{v_c + 2 \rightarrow v_c}$ ($\mathbf{v_c}$ is the upper level number for the central transition). The threshold conditions for all laser transitions correspond to **Fig.3.3**.

For some applications it may be of interest to control the overtone laser spectrum in more complicated manner. For example, it might be desirable to maximize the laser efficiency for several neighboring transitions. It is known from publications (Belykh et al, 1995) that, as a rule, growth of the number of the transitions involved in lasing process is followed by the laser pulse energy increase. This effect was studied by us numerically. Taking the threshold gain for the selected range of frequencies the same as in described above calculations, the results are presented in **Figs.3.5** and **3.6**. It is worth to note that the needed selective resonator may be constructed using a multilayer filter. For lasing on three neighboring vibrational transitions the spectral band of this filter should be about 200 cm^{-1} and for five transitions about 300 cm^{-1}. In **Figs.3.5** and **3.6** the total laser efficiency is shown as a function of the number of the central level, v_c. In particular, the energy corresponding to the number v_c in **Fig.3.5** includes transitions: $v_c \rightarrow v_c - 2$, $v_c - 1 \rightarrow v_c - 3$ and $v_c + 1 \rightarrow v_c - 1$, while in **Fig.3.6** it includes transitions: $v_c \rightarrow v_c - 2$, $v_c - 2 \rightarrow v_c - 4$, $v_c - 1 \rightarrow v_c - 3$, $v_c + 1 \rightarrow v_c - 1$, $v_c + 2 \rightarrow v_c$. It is seen that in each spectral window including three transitions the energy is about two times higher than in the single-frequency mode while for the window containing five transitions the energy is three times higher. It is worth to note that the distribution of the energy over the transitions within one window is as a rule non-uniform being maximum at the lower transitions. It may result in increase of the single-line efficiency in comparison with the single-frequency selection mode. It means that lasing on higher lying transitions may increase the energy in the desired transition and this is in accordance with (Anan'ev et al, 1987; Belykh et al, 1995). This is illustrated in **Fig.3.7**, where the laser efficiency for the lowest transition of the five-transition group is plotted as a function of its number. Comparing these results with that presented in **Fig.3.3** for the simple single-frequency mode demonstrates that for some transitions the resulting efficiency may increase up to 20-30%.

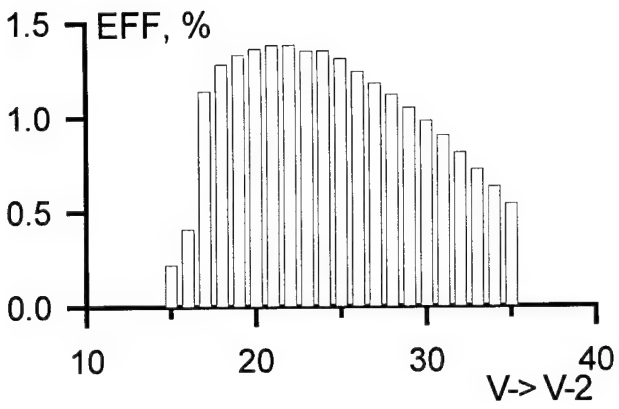

Fig. 3.7. FO CO laser efficiency for the lowest transition in case of lasing on five neighboring vibrational transitions: $v_c - 2 \rightarrow v_c - 4$, $v_c - 1 \rightarrow v_c - 3$, $v_c \rightarrow v_c - 2$, $v_c + 1 \rightarrow v_c - 1$, $v_c + 2 \rightarrow v_c$ (v_c is the upper level of the central transition).
All conditions correspond to **Fig.3.6.**

The comparatively high lasing efficiency, when using the spectral filter with a narrow spectral band, allowing for lasing on several consecutive transitions found in numerical simulations is confirmed by experimental data described in the Section 2.3 (see (Ì 2+Ì 2) in **Figs.2.15** and **2.19**). In experiments laser operation on 5 neighboring transitions (an energy containing in other laser transitions may be neglected) was realized with the efficiency of 5%. The higher than predicted in **Fig.3.6** laser efficiency is explained by lower cavity losses achieved in experiments with multilayer mirrors. This fact emphasizes once more the importance to have a high-quality optical cavity in the FO CO laser with simultaneous suppression of lasing in the fundamental band.

The theoretical analysis presented here showed the possibilities to control the spectral content of the overtone CO laser radiation. The numerical code developed can be used for further simulations of parameter dependencies for the FO CO laser with the laser spectrum control.

Theoretical data demonstrated for FO CO laser efficiency to be strongly dependent on a quality of a diffraction grating. A proposal on a choice of the grating is given in **Appendix IV**.

4.EXTENSION OF THE THEORETICAL MODEL

To evaluate theoretically optimum conditions for the FO CO laser operation our model should be modified by addition of a block describing balance of charged particles (electrons and ions) in plasma of the discharge. In fact, two important from the point of view of laser efficiency factors (the reduced electric field strength, E/N and pumping pulse duration at the given gas density and temperature) result from a compromise between the necessity to increase the pump power as far as possible and appearance of a discharge instability leading to formation of the arc. The instability mechanism is not known for the conditions of the FO CO laser. It is clear that it is inherently coupled with some processes in the electron number balance which give a positive feedback for electron number density growth. Extension of the model onto the plasma chemical kinetics allows also to predict characteristics of different kinds of the self-sustained discharge: dc pulsed and continuos discharge; RF discharge and so on. These are the major reasons for extension of the present kinetic model.

In our previous report (Ionin et al, 1997) a detailed vibration kinetic model for the FO CO laser was described. In that model discharge characteristics were taken from experiments including a discharge power density, and an electric field strength. In fact, discharge characteristics are controlled by processes in plasma: ionization by fast electrons of a beam; attachment to small impurities; electron- and ion-ion recombination; ionization processes including Penning-like ionization in collisions of excited molecules and step-wise ionization also. To describe these effects the model should be strongly modified by adding kinetic equations for chemically active species produced by the discharge in the gas. Among these species the most important for discharge stability are electronically excited molecules. In many experiments it was demonstrated earlier that there exists a limit to the reduced electric field strength, E/N, applied to the discharge. This limit is put by development of an instability followed by formation of high-current arc which can destroy elements of a discharge construction. The discharge current in the EBCD usually is regulated by the e-beam current while keeping constant the high voltage applied to the discharge gap. However, in this situation the instability can be developed after the e-beam current termination. In fact, exactly this process limits the voltage applied. From the other hand, the lower E/N, the lower fraction of the electric power goes to excitation of molecular vibrations. It means that optimum conditions for the effective operation of the FO CO laser are governed by discussed processes. It explains our interest to studying the problem of the discharge instability.

On the way to our goal, it is necessary to extend kinetic description to processes controlling plasma density and ion composition. Practically, we need to modify seriously our program package adding a new subroutine and organizing links providing the real-time information exchange between existing part of the package and that of new developed.

At present, there is no reliable information about processes for electronically excited molecules. This makes the problem of data accumulation a non trivial one. Generally, the kinetic part of the program is governed by a code generator of equations operating on the basis of symbolic equations and a data base containing information about all necessary kinetic coefficients. Our program gives also an opportunity to analyze processes ordering them over their influence on populations of a chosen species. These properties of our code make it particularly valuable in situations of scarce information about kinetic coefficients and their dependence on gas temperature. To elucidate the usage of the program package, an opportunity to work in an interactive mode was offered. It allows us to introduce easily

necessary modifications into the list of the processes included in the model and change their rate coefficients.

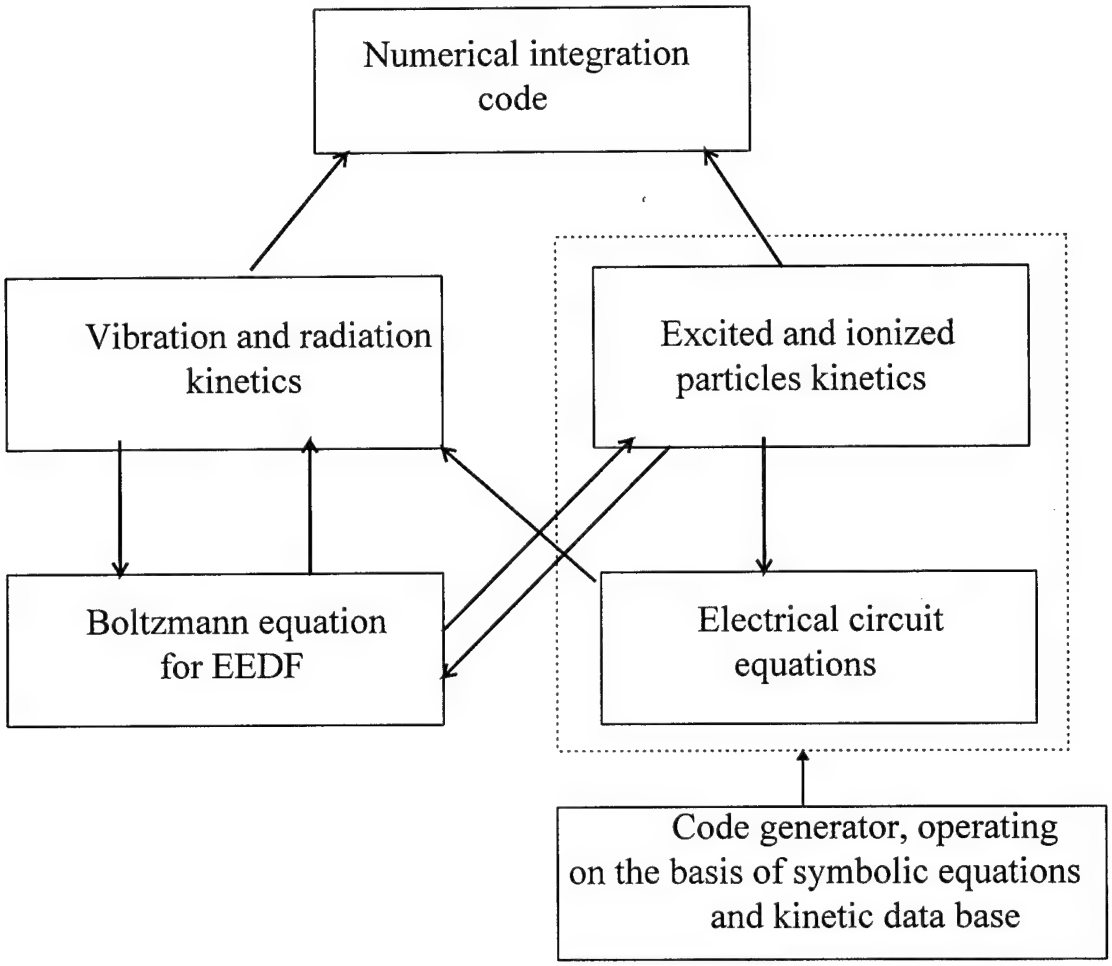

Fig.4.1. Diagram of numerical subroutines and links between them. Dashed box combines the interactive part of the code.

The structure of our program package is illustrated in **Fig.4.1**. It consists of two large blocks: the first, having existed earlier, includes the description of the vibration kinetics and laser dynamics; the second, operating in the interactive mode, includes the description of the plasma chemical processes. The sequence of operations after the start of the program is the following. Initially, the numerical FORTRAN code is generated for solving a system of ordinary differential equations. At this step, the input files with the list of kinetic equations in a symbolic form (see **Table 4.1**) and data on correspondent kinetic coefficients and reaction energy balance are necessary. For processes, where the plasma electrons are involved the correspondent cross sections should be known, because in this case the kinetic coefficients are calculated from the electron Boltzmann equation. The opportunity is reserved to define independently these kinetic coefficients because of lack of information on the needed cross sections. In fact, this code generating differential equations defines mathematical operators for calculations of the right-hand parts of the equations and calculates the elements of Jacoby matrix

necessary for integration of the equation system. Historically, processes with vibrational excited molecules are placed in both blocks necessitating to provide co-ordination between files in different blocks containing enumeration of reactive species. Additionally to the described above kinetic blocks, the differential equation for the electric circuit is generated also.

On the second step, the numerical integration of both parts of kinetic equations in parallel with the electron Boltzmann equation and electric circuit equation is realized. As the code output, laser multi-frequency radiation intensity, populations of different species including vibrational excited molecules and plasma parameters are found as functions of time.

To analyze the discharge stability, it is necessary to take into account different ways in which vibrational excitation may impact on processes of ionization in the EBCD. These are direct and indirect ones. To the direct influence on the ionization, one can ascribe the process of associative ionization in collisions of partners one of which is CO or N_2 molecule on high vibrational level. The existence of processes of this sort is proved by experiments with optical pumping of CO molecules by resonant radiation (Flament et al, 1992). Implicitly, the vibrational excitation may influence on the ionization rate through the deformation of the electron energy distribution function (EEDF). It is known that at the fixed E/N value due to the growth of the vibrational energy a high-energy tail of the EEDF appears. The second potentially important process is the energy transfer process (V-E exchange) from vibrations to electronically excited levels. Electronic metastables produced in such a process may participate further in collisions with other excited molecules resulting in ionization. Moreover, some new reactive channels became open when one of the collision partners is vibrational excited. To calculate correctly plasma density all these processes should be included in the model.

In **Fig. 4.2** an energy diagram is presented where electronically excited molecules and ions are included. The only lowest electronic metastable levels for N_2 and CO having long radiative life-time and stable against quenching by heavy particles are shown. They play a particular role in possible ionization mechanisms. Taking into account that in the EBCD plasma electrons have quite a low mean energy (about 1 eV) excitation of higher lying electronic levels may be neglected.

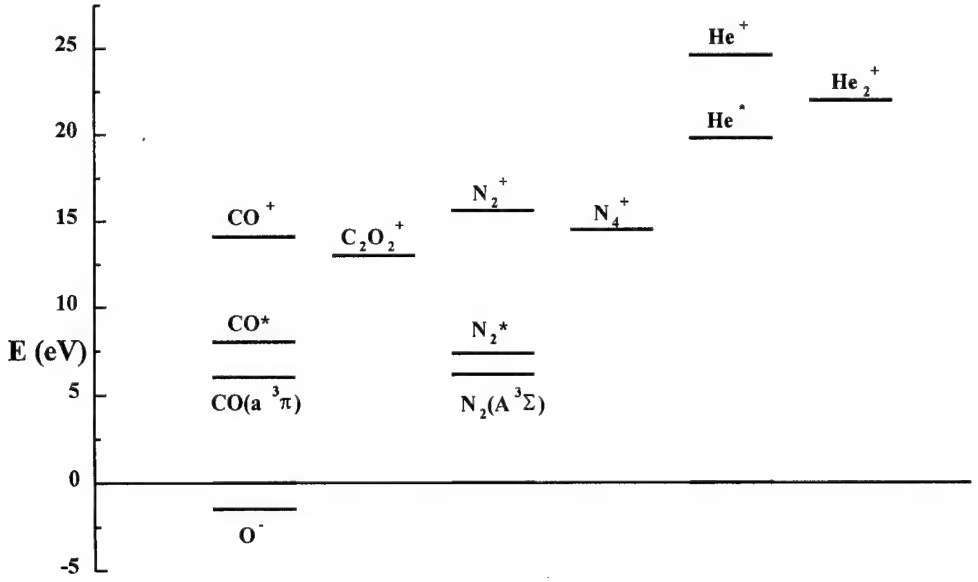

Fig.4.2. Energy diagram for species included in the model

Principally, the program package developed by us can be employed in solving many problems among which are plasma chemistry in closed-cycle electric-discharge excited lasers, a role of E-V energy exchange as in discharge plasma as in gas optically pumped by the resonance radiation and stability of different forms of the electric discharge. Our purpose is the investigation into dominant mechanism of the instability in the EBCD. To start with, we restrict the number of processes included in the model leaving only most important in our opinion. The correspondent data on kinetic coefficients were taken from (Alexandrov et al, 1985; Berdyshev et al, 1988, 1989; Grigor'yan et al, 1992; Ionikh et al, 1986; Polak et al, 1979). The list of these processes is presented in **Table 4.1**.

Table 4.1. The main plasma-chemical processes included in the model

1. $CO + e \rightarrow CO(a^3\pi) + e$	16. $N_2^* + e \rightarrow N_2^+ + e + e$
2. $CO + e \rightarrow CO^* + e$	17. $N_2^+ + e \rightarrow N^* + N$
3. $CO + e \rightarrow CO^+ + e + e$	18. $He + e \rightarrow He^* + e$
4. $CO(a^3\pi) + e \rightarrow CO^+ + e + e$	19. $He + e \rightarrow He^+ + e + e$
5. $CO^* + e \rightarrow CO^+ + e + e$	20. $He^* + e \rightarrow He^+ + e + e$
6. $CO^* + CO^* \rightarrow CO^+ + CO + e$	21. $He_2^+ + e \rightarrow He^* + He$
7. $CO^* + CO(v>v_0) \rightarrow CO^+ + CO + e$	22. $CO^+ + CO + M \rightarrow C_2O_2^+ + M$
8. $CO^+ + e \rightarrow C + O$	23. $N_2^+ + N_2 + M \rightarrow N_4^+ + M$
9. $C_2O_2^+ + e \rightarrow CO(v) + CO(v)$	24. $He^+ + He + M \rightarrow He_2^+ + M$
10. $CO + e \rightarrow C + O(-)$	25. $He^* + CO \rightarrow CO^+ + He$
11. $Fe(CO)_5 + e \rightarrow Fe(CO)_5(-) + e$	26. $He^* + N_2 \rightarrow N_2(+) + He$
12. $N_2 + e \rightarrow N_2(A^3\Sigma) + e$	27. $O(-) + CO \rightarrow CO_2 + e$
13. $N_2 + e \rightarrow N_2^* + e$	28. $CO(a^3\pi) + CO \rightarrow CO(V) + CO$
14. $N_2 + e \rightarrow N_2^+ + e + e$	29. $CO(a^3\pi) + CO \rightarrow CO_2 + C$
15. $N_2(A^3\Sigma) + e \rightarrow N_2^+ + e + e$	30. $N_2(A^3\Sigma) + N_2 \rightarrow N_2(V) + N_2$

5. CONCLUSIONS

1. Application of the new intracavity spectral filter made of fused silica with a thickness of 0.4 mm results in an increase of FO CO laser efficiency and SOE up to 5.5% and 20 J/l·Amagat, respectively, and spectral band broadening up to 3.6 μm.

2. Theoretical calculations, being in rather good agreement with the experimental results, predict for FO CO laser efficiency and SOE to be up to 15-20% and 50-80 J/l·Amagat provided by a decrease of intracavity useless optical losses.

3. Application of various combination of dielectric mirrors results in further extension of pulsed FO CO laser spectrum up to ~4.0 μm and down to 2.5 μm, output efficiency being 5% for FO CO laser with suppressed FB lasing.

4. Theoretical calculations, taking into account the useless optical losses introduced by the dielectric mirrors, are quite in a good agreement with experimental data on energetic and spectral characteristics of FO CO laser with suppressed FB lasing.

5. FO CO laser spectrum can be tuned by using spectral dielectric mirrors, limiting FO CO lasing in a given spectral interval.

6. Dielectric mirrors (with high reflectivity in FO band and low reflectivity in FB) with quite a low absorption, and scattering, and high threshold of optical damage are needed for an achievement of high FO CO laser efficiency up to 10-20%.

7. Theoretically, a comparative study of FO CO laser spectral characteristics was made by using of different frequency selection methods. It was shown, that the laser efficiency for the given transition depends strongly not only on the threshold gain, but also on the spectral selectivity of the laser cavity. In particular, the efficiency for the lowest transition in the free-running mode turned out to be higher than in the cavity selecting this single transition.

8. Generally, for free-running FO CO laser spectrum, one can see two alternating sequences of spectral lines competing each other. Within the same sequence, it is theoretically observed an effect of a co-operative enhancement of the lines. However, only for the lowest transition this effect is strong enough to increase efficiency above that of single frequency selective lasing.

9. It was found, that the same effect of the co-operative enhancement strictly works in case, as the selective cavity allows for lasing within a given spectral interval containing several laser transitions. As a result, the lowest transition in the allowed spectral window (containing 3 or 5 vibrational transitions) has the efficiency higher than it is achievable in a single-frequency selective cavity with equal losses. In conditions studied, this efficiency increase can be up to 30%. This predicted effect correlates with experimental results obtained with the resonator formed by two multilayer mirrors.

10. The developed earlier kinetic package was advanced further by inclusion additional subroutines calculating plasma chemical kinetic equations, the necessary data base for kinetic coefficients and a generator of kinetic equations on the base of symbolic kinetic equations. The last part was made operating in an interactive mode. Additional subroutines together with existing earlier form a complete package with common input and output. The minimum list of plasma chemical reactions necessary to describe self-consistently plasma balance in the EBCD is also presented.

6. ACKNOWLEDGMENTS

Authors are grateful to Mrs. N.Ionina and Mr. M.Minkovsky for their assistance. The research was supported by EOARD and AFRL (USA).

7. REFERENCES

Alexandrov N.L., Kochetov I.V., Napartovich A.P., 1985, Teplofiz Vys. Temp., v.23, 849.

Anan'ev V.Yu., Danilychev V.A., Ionin A.A. et al, 1987, Kvantovaya Electronika, v.14, 1974.

Belykh A.D., Gurashvili V.A., Napartovich A.P. et al, 1995, Kvantovaya Electronika, v.22, 333.

Berdyshev A.V., Golovin A.S., Gurashvili V.A. et al, 1989, Fizika Plazmy, v.15, 335.

Berdyshev A.V., Kochetov I.V., Napartovich A.P., 1988, Fizika Plazmy, v.14, 742.

Flament C., George T., Meister K.A. et al., 1992, Chemical Physics, v.163, 241.

Grigor'yan G.M., Ionikh Y.Z., Kochetov I.V. et al, 1992, J. Phys. D: Appl. Phys.,v.25, 1064.

Guelachvili G., Villeneuve D., Farrrenq R. et al, 1983, J. Mol. Spectr., v.98, 64.

Ionikh Y.Z., Kuranov A.L., Lobanov A.N. et al, 1986, Opt. Spectrosc., v.60, 444.

Ionin A., Galushkin M., .Kotkov A., Mitin K. et al, 1996, "Degenerate four-wave mixing and phase conjugation of molecular mid-IR lasers radiation in their inverted media", Scientific report of the Lebedev Institute on Contract SPC-95-4043 with EOARD.

Ionin A., Napartovich A., Kotkov A., Kurnosov A. et al, 1997, "Experimental and Theoretical Study of First Overtone Carbon Monoxide Laser Physics", Scientific Report of the Lebedev Institute on Contract SPC-97-4014 with EOARD.

Polak L.S., Sergeev P.A. Slovetsky D.I., 1979, Teplofiz. Vys. Temp., v.43, 1464.

APPENDIX I. Spectral characteristics of fused silica filters

The thick filter plate had the thickness 1.9 mm while the thin filter plate was of thickness 0.41 mm with the wedge $\theta = 0.0004$. With help of the spectrophotometer "Perkin-Elmers G983" spectral dependencies for transmission and reflection coefficients of old and new spectral filters were measured. It allows us to find with a good accuracy the dispersion of the refractive index and absorption for both filters in the spectral range 2.0-4.0 μm. As a result, cavity losses associated with absorption and reflection from the filter plate for every spectral line of the FO CO laser may be calculated for a given decline angle of the filter plate relatively to the optical axis. The results are presented in the **Tables AI.1** and **AI.2** for two values of the incidence angle, each being the optimum one for thin and thick filter plates correspondingly. In the first and second columns of the tables the upper vibrational and rotational numbers of the overtone transition are listed. In the third column the wavelength of this transition is placed. Columns under the title "intracavity" contain computed overall cavity losses including absorption in metal cavity mirrors, for both plates. "Absorption losses" accounts for absorption in the plate, and "output coupling" gives the percentage of the reflected from the plate radiation.

Table. AI.1.

The intracavity, absorption and output coupling losses of fused silica plates for incidence angle 27°

V	J	λ, (μm)	intracavity losses, %		absorption losses, %		output coupling, %	
			thick	thin	thick	thin	thick	thin
6	10	2. 494	10.62	10.47	0.2016	0.04248	8.032	8.042
6	11	2.496	10.64	10.47	0.221	0.04656	8.031	8.042
6	12	2.499	10.63	10.45	0.2414	0.05087	7.998	8.01
6	13	2.502	10.65	10.46	0.262	0.05522	7.996	8.009
6	14	2.505	10.64	10.43	0.2837	0.05979	7.963	7.976
7	10	2.526	10.68	10.35	0.4474	0.09437	7.858	7.879
7	11	2.529	10.69	10.34	0.4686	0.09885	7.857	7.879
7	12	2.532	10.67	10.31	0.4904	0.1034	7.824	7.847
7	13	2.535	10.67	10.29	0.512	0.108	7.823	7.848
7	14	2.538	10.69	10.29	0.5335	0.1126	7.822	7.848
8	10	2.56	10.68	10.17	0.6847	0.1445	7.72	7.753
8	11	2.563	10.65	10.13	0.7019	0.1482	7.688	7.721

8	12	2.566	10.67	10.13	0.7189	0.1518	7.687	7.721
8	13	2.569	10.65	10.1	0.7357	0.1554	7.654	7.689
8	14	2.572	10.66	10.1	0.752	0.1588	7.654	7.689
9	10	2.594	10.67	10.03	0.8553	0.1807	7.585	7.625
9	11	2.597	10.69	10.04	0.8662	0.183	7.585	7.625
9	12	2.60	10.66	10.01	0.8774	0.1854	7.553	7.593
9	13	2.603	10.67	10.01	0.8876	0.1875	7.552	7.593
9	14	2.606	10.68	10.01	0.8978	0.1897	7.551	7.593
10	10	2.629	10.63	9.909	0.9611	0.2031	7.52	7.564
10	11	2.632	10.63	9.91	0.9672	0.2044	7.519	7.564
10	12	2.635	10.67	9.944	0.9734	0.2057	7.55	7.595
10	13	2.638	10.69	9.954	0.9797	0.2071	7.55	7.595
10	14	2.642	10.71	9.974	0.9857	0.2083	7.549	7.594
11	10	2.665	10.8	10.02	1.032	0.2182	7.577	7.625
11	11	2.668	10.83	10.05	1.039	0.2196	7.608	7.657
11	12	2.672	10.81	10.02	1.046	0.2212	7.609	7.658
11	13	2.675	10.79	10.01	1.054	0.2229	7.609	7.658
11	14	2.678	10.78	9.989	1.063	0.2247	7.61	7.659
12	10	2.702	10.95	10.09	1.153	0.244	7.667	7.721
12	11	2.705	10.97	10.09	1.169	0.2472	7.666	7.72
12	12	2.708	10.99	10.11	1.186	0.2508	7.664	7.72
12	13	2.712	11.01	10.11	1.204	0.2547	7.663	7.72
12	14	2.715	11.03	10.11	1.223	0.2588	7.662	7.719
13	10	2.74	11.27	10.2	1.424	0.3016	7.615	7.682
13	11	2.743	11.3	10.21	1.456	0.3084	7.613	7.681
13	12	2.746	11.33	10.22	1.489	0.3153	7.611	7.681
13	13	2.75	11.36	10.22	1.525	0.323	7.61	7.681
13	14	2.753	11.38	10.21	1.563	0.3311	7.608	7.681
14	10	2.779	11.75	10.31	1.924	0.4084	7.585	7.675
14	11	2.782	11.79	10.32	1.978	0.4198	7.582	7.675
14	12	2.785	11.84	10.32	2.033	0.4316	7.58	7.674
14	13	2.789	11.88	10.32	2.091	0.4441	7.576	7.674
14	14	2.792	11.93	10.32	2.153	0.4573	7.573	7.674
15	10	2.819	12.38	10.38	2.679	0.5702	7.577	7.702
15	11	2.822	12.43	10.39	2.745	0.5844	7.573	7.702
15	12	2.825	12.49	10.39	2.813	0.5991	7.57	7.701
15	13	2.829	12.55	10.4	2.884	0.6144	7.566	7.701
15	14	2.832	12.65	10.44	2.953	0.6293	7.593	7.731
16	10	2.859	13.23	10.62	3.5	0.7476	7.59	7.754
16	11	2.863	13.28	10.63	3.562	0.7611	7.586	7.754
16	12	2.866	13.33	10.63	3.625	0.7747	7.583	7.754
16	13	2.87	13.42	10.67	3.688	0.7883	7.611	7.785

16	14	2.873	13.46	10.67	3.749	0.8016	7.607	7.785
17	10	2.901	13.9	10.76	4.209	0.9017	7.612	7.812
17	11	2.905	13.94	10.77	4.26	0.9128	7.609	7.811
17	12	2.908	13.99	10.78	4.311	0.924	7.606	7.81
17	13	2.912	14.04	10.79	4.362	0.9351	7.603	7.81
17	14	2.915	14.09	10.8	4.413	0.9462	7.6	7.809
18	10	2.944	14.49	10.92	4.785	1.028	7.576	7.802
18	11	2.948	14.52	10.92	4.825	1.036	7.574	7.802
18	12	2.951	14.54	10.92	4.865	1.045	7.572	7.802
18	13	2.955	14.57	10.92	4.905	1.054	7.57	7.802
18	14	2.958	14.61	10.93	4.945	1.063	7.567	7.801
19	10	2.988	14.83	10.93	5.232	1.126	7.521	7.767
19	11	2.992	14.84	10.93	5.261	1.132	7.519	7.767
19	12	2.995	14.85	10.92	5.29	1.139	7.518	7.767
19	13	2.999	14.87	10.91	5.319	1.145	7.517	7.767
19	14	3.003	14.85	10.87	5.346	1.151	7.485	7.736
20	10	3.033	14.87	10.77	5.509	1.187	7.449	7.706
20	11	3.037	14.88	10.76	5.52	1.189	7.449	7.707
20	12	3.041	14.88	10.76	5.531	1.192	7.449	7.707
20	13	3.045	14.88	10.75	5.542	1.194	7.448	7.707
20	14	3.048	14.89	10.75	5.549	1.196	7.448	7.707
21	10	3.08	14.85	10.7	5.573	1.201	7.417	7.676
21	11	3.084	14.85	10.7	5.573	1.201	7.417	7.676
21	12	3.087	14.81	10.65	5.571	1.201	7.387	7.645
21	13	3.091	14.8	10.64	5.568	1.2	7.388	7.646
21	14	3.095	14.79	10.64	5.564	1.199	7.388	7.646
22	10	3.128	14.65	10.54	5.517	1.189	7.363	7.617
22	11	3.131	14.63	10.52	5.51	1.187	7.364	7.618
22	12	3.135	14.61	10.5	5.507	1.186	7.365	7.619
22	13	3.139	14.58	10.47	5.501	1.185	7.366	7.62
22	14	3.143	14.55	10.45	5.491	1.183	7.368	7.621
23	10	3.177	14.48	10.45	5.404	1.164	7.309	7.556
23	11	3.181	14.48	10.46	5.393	1.161	7.309	7.555
23	12	3.184	14.47	10.45	5.379	1.158	7.31	7.556
23	13	3.188	14.45	10.45	5.361	1.154	7.311	7.556
23	14	3.193	14.43	10.44	5.343	1.15	7.312	7.557
24	10	3.227	14.05	10.21	5.139	1.105	7.268	7.501
24	11	3.231	14.02	10.2	5.107	1.098	7.27	7.502
24	12	3.235	13.98	10.19	5.074	1.091	7.272	7.502
24	13	3.239	13.95	10.18	5.038	1.083	7.274	7.503
24	14	3.243	13.9	10.16	5.002	1.075	7.276	7.504
25	10	3.279	13.59	10.06	4.724	1.014	7.263	7.476

25	11	3.283	13.57	10.05	4.702	1.009	7.264	7.477
25	12	3.287	13.55	10.05	4.684	1.005	7.265	7.477
25	13	3.292	13.53	10.04	4.669	1.002	7.266	7.477
25	14	3.296	13.52	10.03	4.658	0.9999	7.267	7.478
26	10	3.333	13.62	10.02	4.816	1.034	7.26	7.477
26	11	3.337	13.7	10.06	4.866	1.045	7.287	7.508
26	12	3.341	13.77	10.08	4.927	1.059	7.283	7.507
26	13	3.345	13.84	10.1	4.996	1.074	7.279	7.506
26	14	3.35	13.92	10.12	5.076	1.091	7.274	7.505
27	10	3.388	14.89	10.45	5.952	1.285	7.282	7.554
27	11	3.392	14.96	10.44	6.061	1.309	7.245	7.521
27	12	3.396	15.06	10.45	6.176	1.334	7.239	7.52
27	13	3.401	15.17	10.47	6.298	1.361	7.232	7.518
27	14	3.405	15.28	10.49	6.427	1.39	7.225	7.517
28	10	3.445	16.87	10.71	8.265	1.802	7.002	7.37
28	11	3.449	17.17	10.77	8.58	1.873	6.984	7.366
28	12	3.453	17.5	10.85	8.928	1.952	6.965	7.361
28	13	3.458	17.84	10.9	9.316	2.04	6.914	7.325
28	14	3.462	18.24	10.99	9.737	2.137	6.89	7.32
29	10	3.503	22.62	11.97	14.41	3.229	6.602	7.228
29	11	3.507	23.17	12.1	14.98	3.366	6.57	7.221
29	12	3.512	23.73	12.23	15.57	3.509	6.538	7.213
29	13	3.517	24.3	12.37	16.18	3.657	6.504	7.205
29	14	3.521	24.9	12.51	16.81	3.81	6.47	7.196
30	10	3.563	29.91	13.68	22.2	5.164	6.096	7.03
30	11	3.568	30.39	13.81	22.7	5.295	6.069	7.023
30	12	3.573	30.85	13.91	23.21	5.428	6.016	6.985
30	13	3.577	31.32	14.03	23.7	5.557	5.99	6.978
30	14	3.582	31.78	14.15	24.19	5.684	5.964	6.971
31	10	3.626	36.45	15.4	29.13	7.025	5.65	6.836
31	11	3.63	37.1	15.58	29.8	7.215	5.615	6.826
31	12	3.635	37.8	15.78	30.55	7.425	5.576	6.815
31	13	3.64	38.58	15.99	31.38	7.662	5.533	6.802
31	14	3.645	39.4	16.22	32.25	7.913	5.488	6.789
32	10	3.69	47.73	18.79	41.03	10.6	5.032	6.642
32	11	3.695	48.53	19.05	41.89	10.89	4.966	6.597
32	12	3.7	49.32	19.32	42.72	11.16	4.924	6.582
32	13	3.705	50.07	19.57	43.51	11.42	4.883	6.568
32	14	3.71	50.78	19.81	44.26	11.68	4.845	6.554

Table. AI.2.

The intracavity absorption and output coupling losses of fused silica plates for incidence angle 33 °								
V	*J*	λ,(μm)	intracavity losses, %		absorption losses, %		output coupling, %	
			thick	thin	thick	thin	thick	thin
6	13	2.502	8.926	8.722	0.2713	0.05718	6.271	6.281
6	14	2.505	8.921	8.699	0.2937	0.06191	6.243	6.254
7	10	2.526	8.983	8.633	0.4633	0.09772	6.155	6.172
7	11	2.529	8.994	8.628	0.4853	0.1024	6.154	6.172
7	12	2.532	8.98	8.596	0.5077	0.1071	6.126	6.145
7	13	2.535	8.982	8.582	0.5301	0.1118	6.126	6.146
7	14	2.538	8.994	8.577	0.5525	0.1166	6.125	6.146
8	10	2.560	9.007	8.472	0.7089	0.1497	6.039	6.065
8	11	2.563	8.988	8.439	0.7268	0.1535	6.012	6.039
8	12	2.566	9.005	8.443	0.7444	0.1572	6.011	6.039
8	13	2.569	8.995	8.420	0.7618	0.1609	5.984	6.012
8	14	2.572	9.002	8.414	0.7787	0.1645	5.983	6.012
9	10	2.594	9.032	8.363	0.8856	0.1871	5.926	5.958
9	11	2.597	9.043	8.365	0.8969	0.1895	5.926	5.958
9	12	2.600	9.027	8.341	0.9085	0.192	5.899	5.931
9	13	2.603	9.038	8.343	0.9191	0.1942	5.898	5.931
9	14	2.606	9.048	8.345	0.9296	0.1965	5.898	5.931
10	10	2.629	9.000	8.248	0.9952	0.2104	5.871	5.906
10	11	2.632	9.006	8.249	1.002	0.2117	5.871	5.906
10	12	2.635	9.038	8.277	1.008	0.2131	5.897	5.933
10	13	2.638	9.054	8.287	1.014	0.2145	5.896	5.933
10	14	2.642	9.079	8.308	1.021	0.2158	5.895	5.932
11	10	2.665	9.161	8.353	1.069	0.226	5.919	5.958
11	11	2.668	9.185	8.372	1.076	0.2274	5.946	5.985
11	12	2.672	9.164	8.346	1.083	0.229	5.946	5.985
11	13	2.675	9.153	8.328	1.091	0.2308	5.946	5.986
11	14	2.678	9.143	8.312	1.101	0.2327	5.947	5.986
12	10	2.702	9.305	8.403	1.194	0.2526	5.995	6.038
12	11	2.705	9.32	8.406	1.21	0.256	5.994	6.038
12	12	2.708	9.346	8.419	1.228	0.2597	5.993	6.038
12	13	2.712	9.364	8.423	1.246	0.2637	5.992	6.038
12	14	2.715	9.384	8.427	1.267	0.268	5.991	6.037

13	10	2.740	9.640	8.527	1.474	0.3123	5.952	6.006
13	11	2.743	9.671	8.534	1.507	0.3193	5.951	6.006
13	12	2.746	9.704	8.541	1.541	0.3265	5.949	6.005
13	13	2.750	9.730	8.539	1.579	0.3345	5.948	6.005
13	14	2.753	9.759	8.538	1.618	0.3429	5.946	6.005
14	10	2.779	10.15	8.642	1.992	0.4229	5.928	6.000
14	11	2.782	10.19	8.644	2.048	0.4347	5.926	6.000
14	12	2.785	10.23	8.647	2.105	0.4469	5.924	6.000
14	13	2.789	10.28	8.650	2.165	0.4598	5.921	6.000
14	14	2.792	10.33	8.653	2.229	0.4735	5.918	5.999
15	10	2.819	10.8	8.708	2.773	0.5904	5.922	6.023
15	11	2.822	10.85	8.713	2.841	0.6051	5.919	6.023
15	12	2.825	10.91	8.718	2.912	0.6204	5.916	6.022
15	13	2.829	10.97	8.724	2.985	0.6362	5.913	6.022
15	14	2.832	11.07	8.765	3.057	0.6517	5.936	6.048
16	10	2.859	11.67	8.947	3.622	0.7741	5.935	6.068
16	11	2.863	11.73	8.951	3.687	0.7881	5.932	6.067
16	12	2.866	11.78	8.955	3.752	0.8022	5.93	6.067
16	13	2.87	11.86	8.986	3.817	0.8163	5.953	6.093
16	14	2.873	11.91	8.99	3.88	0.83	5.95	6.093
17	10	2.901	12.36	9.079	4.356	0.9336	5.955	6.116
17	11	2.905	12.41	9.09	4.408	0.9452	5.953	6.116
17	12	2.908	12.46	9.101	4.461	0.9567	5.95	6.115
17	13	2.912	12.51	9.112	4.514	0.9682	5.948	6.115
17	14	2.915	12.56	9.123	4.566	0.9797	5.945	6.114
18	10	2.944	12.97	9.25	4.951	1.064	5.926	6.109
18	11	2.948	13	9.25	4.993	1.073	5.924	6.108
18	12	2.951	13.03	9.249	5.034	1.082	5.923	6.108
18	13	2.955	13.06	9.249	5.076	1.091	5.921	6.108
18	14	2.958	13.1	9.257	5.117	1.1	5.919	6.108
19	10	2.988	13.33	9.265	5.413	1.166	5.88	6.079
19	11	2.992	13.35	9.262	5.444	1.172	5.879	6.079
19	12	2.995	13.36	9.25	5.474	1.179	5.878	6.079
19	13	2.999	13.38	9.247	5.504	1.186	5.877	6.079
19	14	3.003	13.37	9.207	5.532	1.192	5.851	6.053
20	10	3.033	13.4	9.113	5.7	1.229	5.821	6.028
20	11	3.037	13.4	9.106	5.712	1.231	5.82	6.028
20	12	3.041	13.4	9.1	5.723	1.234	5.82	6.028
20	13	3.045	13.41	9.093	5.734	1.236	5.82	6.028
20	14	3.048	13.41	9.094	5.742	1.238	5.819	6.028
21	10	3.08	13.38	9.045	5.767	1.243	5.794	6.002
21	11	3.084	13.38	9.045	5.767	1.243	5.794	6.002

21	12	3.087	13.35	9.008	5.765	1.243	5.768	5.976
21	13	3.091	13.33	8.998	5.761	1.242	5.769	5.976
21	14	3.095	13.33	8.997	5.757	1.241	5.769	5.976
22	10	3.128	13.19	8.895	5.709	1.231	5.748	5.952
22	11	3.131	13.17	8.875	5.702	1.229	5.749	5.953
22	12	3.135	13.15	8.855	5.699	1.228	5.749	5.954
22	13	3.139	13.11	8.826	5.692	1.227	5.75	5.955
22	14	3.143	13.09	8.805	5.682	1.225	5.752	5.955
23	10	3.177	13.03	8.817	5.593	1.205	5.702	5.901
23	11	3.181	13.03	8.824	5.581	1.203	5.702	5.901
23	12	3.184	13.01	8.82	5.566	1.199	5.703	5.901
23	13	3.188	13	8.817	5.547	1.195	5.704	5.901
23	14	3.193	12.97	8.803	5.529	1.191	5.705	5.901
24	10	3.227	12.6	8.584	5.318	1.145	5.667	5.854
24	11	3.231	12.56	8.577	5.285	1.137	5.668	5.855
24	12	3.235	12.52	8.56	5.251	1.13	5.67	5.855
24	13	3.239	12.49	8.552	5.214	1.122	5.672	5.856
24	14	3.243	12.44	8.535	5.176	1.113	5.674	5.856
25	10	3.279	12.12	8.429	4.889	1.05	5.662	5.834
25	11	3.283	12.1	8.424	4.866	1.045	5.663	5.834
25	12	3.287	12.08	8.42	4.847	1.041	5.664	5.834
25	13	3.292	12.06	8.408	4.833	1.038	5.665	5.834
25	14	3.296	12.05	8.406	4.821	1.035	5.665	5.834
26	10	3.333	12.16	8.393	4.984	1.071	5.659	5.834
26	11	3.337	12.23	8.431	5.036	1.082	5.682	5.86
26	12	3.341	12.3	8.454	5.099	1.096	5.679	5.859
26	13	3.345	12.37	8.469	5.171	1.112	5.676	5.859
26	14	3.35	12.46	8.495	5.253	1.13	5.672	5.857
27	10	3.388	13.45	8.816	6.158	1.33	5.68	5.899
27	11	3.392	13.54	8.813	6.271	1.355	5.65	5.871
27	12	3.396	13.64	8.829	6.39	1.382	5.645	5.87
27	13	3.401	13.75	8.847	6.516	1.41	5.639	5.869
27	14	3.405	13.87	8.866	6.649	1.439	5.634	5.868
28	10	3.445	15.55	9.123	8.549	1.866	5.451	5.746
28	11	3.449	15.86	9.194	8.874	1.939	5.436	5.743
28	12	3.453	16.21	9.273	9.234	2.021	5.42	5.739
28	13	3.458	16.57	9.334	9.635	2.113	5.378	5.709
28	14	3.462	16.99	9.43	10.07	2.212	5.359	5.704
29	10	3.503	21.56	10.46	14.89	3.343	5.128	5.63
29	11	3.507	22.13	10.59	15.48	3.485	5.103	5.624
29	12	3.512	22.71	10.73	16.09	3.632	5.076	5.617
29	13	3.517	23.31	10.87	16.72	3.786	5.05	5.611

29	14	3.521	23.93	11.02	17.37	3.944	5.022	5.604
30	10	3.563	29.16	12.27	22.91	5.345	4.721	5.467
30	11	3.568	29.66	12.4	23.43	5.48	4.7	5.462
30	12	3.573	30.14	12.51	23.95	5.618	4.656	5.431
30	13	3.577	30.62	12.63	24.45	5.75	4.635	5.425
30	14	3.582	31.1	12.76	24.95	5.883	4.615	5.419
31	10	3.626	35.95	14.08	30.02	7.268	4.364	5.309
31	11	3.63	36.62	14.27	30.72	7.465	4.336	5.301
31	12	3.635	37.34	14.47	31.48	7.682	4.305	5.292
31	13	3.64	38.15	14.7	32.33	7.927	4.271	5.282
31	14	3.645	39	14.94	33.22	8.186	4.235	5.271
32	10	3.69	47.59	17.61	42.19	10.97	3.875	5.154
32	11	3.695	48.43	17.89	43.07	11.26	3.822	5.117
32	12	3.7	49.23	18.16	43.91	11.54	3.789	5.105
32	13	3.705	50	18.43	44.71	11.81	3.757	5.094
32	14	3.71	50.74	18.68	45.48	12.07	3.726	5.083

APPENDIX II. Spectral characteristics of dielectric mirrors

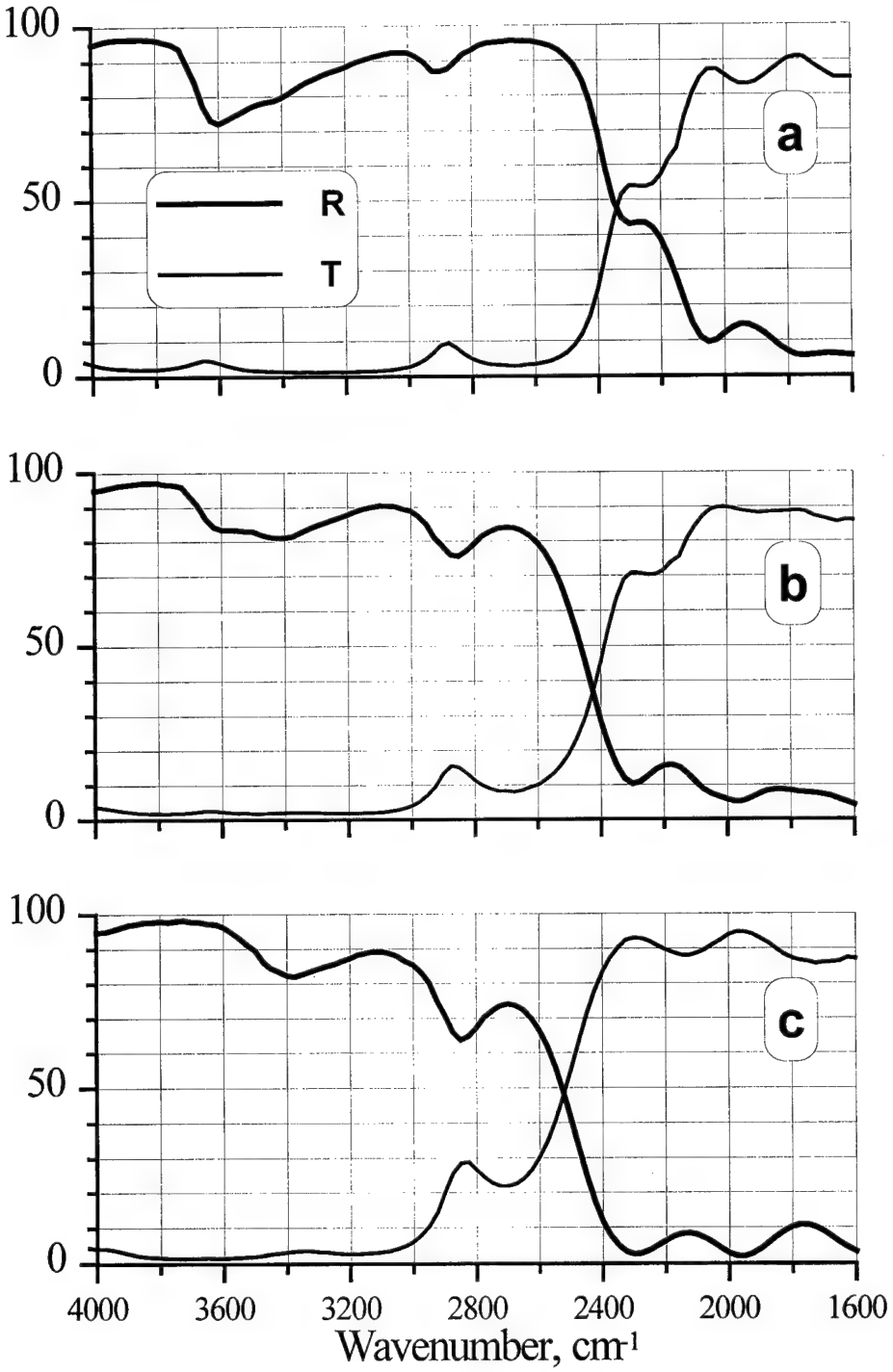

Fig.AII.1. Measured spectral characteristics (reflectivity R and transmittance T in percents) of dielectric mirrors M1 (a) and M2 (c) used in the experiments.
The equivalent characteristics of the combination of the two mirrors $R=(R_1 R_2)^{0.5}$ and $T=(T_1 T_2)^{0.5}$ are presented also (b).

APPENDIX III. Calculated wavelengths and wavenumbers for FO CO laser transitions

Table AIII. *Calculated CO overtone laser wavenumbers in vacuum (cm^{-1}) and wavelengths in ambient air (μm) for different isotopic modifications*

		$^{12}C^{16}O$		$^{13}C^{16}O$		$^{12}C^{18}O$	
v→v-2		1/λ	λ	1/λ	λ	1/λ	λ
6 - 4	P(9)	4013.4528	2.4909 2.5476	3931.0634	2.5431	3924.1654	
	P(10)	4009.1245	2.4936 2.5502	3926.9357	2.5458	3920.0542	
	P(11)	4004.7278	2.4963 2.5530	3922.7439	2.5485	3915.8793	
	P(12)	4000.2626	2.4991 2.5557	3918.4882	2.5513	3911.6408	
	P(13)	3995.7292	2.5019 2.5585	3914.1687	2.5541	3907.3389	
	P(14)	3991.1277	2.5048 2.5614	3909.7855	2.5569	3902.9737	
	P(15)	3986.4583	2.5078 2.5643	3905.3388	2.5598	3898.5452	
	P(16)	3981.7211	2.5107 2.5673	3900.8286	2.5628	3894.0538	
7 - 5	P(9)	3961.4279	2.5236 2.5802	3881.3069	2.5757	3874.5962	
	P(10)	3957.1347	2.5263 2.5829	3877.2119	2.5784	3870.5176	
	P(11)	3952.7730	2.5291 2.5856	3873.0529	2.5812	3866.3753	
	P(12)	3948.3429	2.5320 2.5885	3868.8300	2.5840	3862.1694	
	P(13)	3943.8446	2.5349 2.5913	3864.5433	2.5869	3857.9001	
	P(14)	3939.2782	2.5378 2.5942	3860.1929	2.5898	3853.5674	
	P(15)	3934.6439	2.5408 2.5972	3855.7790	2.5928	3849.1717	
	P(16)	3929.9418	2.5438 2.6002	3851.3017	2.5958	3844.7128	

8 - 6	P(9)	3909.5500	2.5571	3831.6873	2.6091	3825.1631
			2.6135			
	P(10)	3905.2919	2.5599	3827.6251	2.6118	3821.1171
			2.6163			
	P(11)	3900.9652	2.5627	3823.4989	2.6146	3817.0074
			2.6191			
	P(12)	3896.5702	2.5656	3819.3087	2.6175	3812.8341
			2.6220			
	P(13)	3892.1070	2.5686	3815.0548	2.6204	3808.5974
			2.6249			
	P(14)	3887.5757	2.5715	3810.7372	2.6234	3804.2974
			2.6278			
	P(15)	3882.9766	2.5746	3806.3561	2.6264	3799.9342
			2.6309			
	P(16)	3878.3096	2.5777	3801.9117	2.6295	3795.5080
			2.6339			
9 - 7	P(9)	3857.8223	2.5914	3782.2076	2.6432	3775.8691
			2.6476			
	P(10)	3853.5993	2.5942	3778.1782	2.6460	3771.8557
			2.6504			
	P(11)	3849.3077	2.5971	3774.0848	2.6489	3767.7786
			2.6533			
	P(12)	3844.9478	2.6001	3769.9275	2.6518	3763.6379
			2.6562			
	P(13)	3840.5197	2.6031	3765.7063	2.6548	3759.4338
			2.6592			
	P(14)	3836.0236	2.6061	3761.4216	2.6578	3755.1664
			2.6622			
	P(15)	3831.4595	2.6092	3757.0733	2.6609	3750.8359
			2.6653			
	P(16)	3826.8277	2.6124	3752.6616	2.6640	3746.4423
			2.6684			

		$^{12}C^{16}O$		$^{13}C^{16}O$		$^{12}C^{18}O$	
v→v-2		1/λ	λ	1/λ	λ	1/λ	λ
10 - 8	P(9)	3806.2481	2.6265	3732.8708	2.6781	3726.7171	
			2.6825				
	P(10)	3802.0601	2.6294	3728.8742	2.6810	3722.7362	
			2.6854				
	P(11)	3797.8037	2.6323	3724.8136	2.6839	3718.6917	
			2.6883				
	P(12)	3793.4789	2.6353	3720.6890	2.6869	3714.5837	
			2.6913				
	P(13)	3789.0859	2.6384	3716.5007	2.6899	3710.4122	
			2.6943				
	P(14)	3784.6249	2.6415	3712.2488	2.6930	3706.1775	
			2.6974				
	P(15)	3780.0959	2.6447	3707.9333	2.6961	3701.8796	
			2.7005				
	P(16)	3775.4992	2.6479	3703.5545	2.6993	3697.5187	
			2.7037				
11 - 9	P(9)	3754.8303	2.6625	3683.6796	2.7139	3677.7098	
			2.7183				
	P(10)	3750.6774	2.6654	3679.7158	2.7168	3673.7616	
			2.7212				
	P(11)	3746.4560	2.6684	3675.6880	2.7198	3669.7497	
			2.7242				
	P(12)	3742.1663	2.6715	3671.5962	2.7228	3665.6742	
			2.7272				
	P(13)	3737.8085	2.6746	3667.4407	2.7259	3661.5354	
			2.7303				
	P(14)	3733.3826	2.6778	3663.2216	2.7290	3657.3333	
			2.7334				
	P(15)	3728.8888	2.6810	3658.9390	2.7322	3653.0681	
			2.7366				
	P(16)	3724.3273	2.6843	3654.5931	2.7355	3648.7398	
			2.7399				
12 - 10	P(9)	3703.5717	2.6993	3634.6366	2.7505	3628.8498	
			2.7549				
	P(10)	3699.4539	2.7023	3630.7056	2.7535	3624.9342	
			2.7579				
	P(11)	3695.2676	2.7054	3626.7106	2.7565	3620.9549	
			2.7609				

	P(12)	3691.0130	2.7085	3622.6517	2.7596	3616.9121
			2.7640			
	P(13)	3686.6903	2.7117	3618.5290	2.7627	3612.8059
			2.7671			
	P(14)	3682.2995	2.7149	3614.3427	2.7659	3608.6365
			2.7703			
	P(15)	3677.8409	2.7182	3610.0929	2.7692	3604.4039
			2.7736			
	P(16)	3673.3145	2.7215	3605.7798	2.7725	3600.1083
			2.7769			
13 - 11	P(9)	3652.4749	2.7371	3585.7443	2.7880	3580.1396
			2.7924			
	P(10)	3648.3922	2.7401	3581.8460	2.7910	3576.2565
			2.7954			
	P(11)	3644.2410	2.7433	3577.8838	2.7941	3572.3099
			2.7985			
	P(12)	3640.0215	2.7464	3573.8577	2.7973	3568.2997
			2.8016			
	P(13)	3635.7339	2.7497	3569.7679	2.8005	3564.2261
			2.8048			
	P(14)	3631.3783	2.7530	3565.6144	2.8037	3560.0893
			2.8081			
	P(15)	3626.9548	2.7563	3561.3975	2.8071	3555.8894
			2.8114			
	P(16)	3622.4636	2.7597	3557.1172	2.8104	3551.6265
			2.8148			
14 - 12	P(9)	3601.5421	2.7758	3537.0047	2.8264	3531.5811
			2.8308			
	P(10)	3597.4945	2.7789	3533.1392	2.8295	3527.7307
			2.8339			
	P(11)	3593.3784	2.7821	3529.2098	2.8327	3523.8167
			2.8370			
	P(12)	3589.1940	2.7853	3525.2165	2.8359	3519.8391
			2.8402			
	P(13)	3584.9415	2.7886	3521.1595	2.8391	3515.7982
			2.8435			
	P(14)	3580.6210	2.7920	3517.0389	2.8425	3511.6940
			2.8468			
	P(15)	3576.2327	2.7954	3512.8548	2.8459	3507.5268
			2.8502			
	P(16)	3571.7767	2.7989	3508.6074	2.8493	3503.2965
			2.8536			

		$^{12}C^{16}O$		$^{13}C^{16}O$		$^{12}C^{18}O$	
v→v-2		1/λ	λ	1/λ	λ	1/λ	λ
15 - 13	P(9)	3550.7754	2.8155	3488.4198	2.8658	3483.1765	
			2.8701				
	P(10)	3546.7628	2.8186	3484.5871	2.8689	3479.3586	
			2.8733				
	P(11)	3542.6818	2.8219	3480.6905	2.8722	3475.4772	
			2.8765				
	P(12)	3538.5326	2.8252	3476.7300	2.8754	3471.5323	
			2.8797				
	P(13)	3534.3152	2.8286	3472.7058	2.8788	3467.5240	
			2.8831				
	P(14)	3530.0298	2.8320	3468.6180	2.8822	3463.4525	
			2.8864				
	P(15)	3525.6766	2.8355	3464.4668	2.8856	3459.3178	
			2.8899				
	P(16)	3521.2557	2.8391	3460.2522	2.8891	3455.1203	
			2.8934				
16 - 14	P(9)	3500.1762	2.8562	3439.9910	2.9061	3434.9270	
			2.9104				
	P(10)	3496.1987	2.8594	3436.1911	2.9093	3431.1418	
			2.9136				
	P(11)	3492.1528	2.8627	3432.3273	2.9126	3427.2930	
			2.9169				
	P(12)	3488.0387	2.8661	3428.3996	2.9160	3423.3806	
			2.9202				
	P(13)	3483.8564	2.8695	3424.4082	2.9194	3419.4050	
			2.9236				
	P(14)	3479.6062	2.8730	3420.3533	2.9228	3415.3661	
			2.9271				
	P(15)	3475.2881	2.8766	3416.2349	2.9263	3411.2642	
			2.9306				
	P(16)	3470.9024	2.8803	3412.0532	2.9299	3407.0992	
			2.9342				
17 - 15	P(9)	3449.7458	2.8979	3391.7197	2.9475	3386.8341	
			2.9517				
	P(10)	3445.8034	2.9012	3387.9526	2.9508	3383.0814	
			2.9550				
	P(11)	3441.7925	2.9046	3384.1215	2.9541	3379.2652	
			2.9584				

	P(12)	3437.7135	2.9081	3380.2266	2.9575	3375.3855
			2.9618			
	P(13)	3433.5663	2.9116	3376.2680	2.9610	3371.4424
			2.9652			
	P(14)	3429.3512	2.9152	3372.2459	2.9645	3367.4362
			2.9688			
	P(15)	3425.0682	2.9188	3368.1604	2.9681	3363.3669
			2.9723			
	P(16)	3420.7176	2.9225	3364.0115	2.9718	3359.2346
			2.9760			
18 - 16	P(9)	3399.4848	2.9408	3343.6066	2.9899	3338.8984
			2.9941			
	P(10)	3395.5775	2.9441	3339.8722	2.9933	3335.1783
			2.9975			
	P(11)	3391.6017	2.9476	3336.0739	2.9967	3331.3946
			3.0009			
	P(12)	3387.5577	2.9511	3332.2118	3.0001	3327.5475
			3.0043			
	P(13)	3383.4456	2.9547	3328.2860	3.0037	3323.6371
			3.0079			
	P(14)	3379.2655	2.9584	3324.2967	3.0073	3319.6635
			3.0115			
	P(15)	3375.0177	2.9621	3320.2439	3.0109	3315.6268
			3.0151			
	P(16)	3370.7022	2.9659	3316.1279	3.0147	3311.5271
			3.0189			
19 - 17	P(9)	3349.3935	2.9847	3295.6520	3.0334	3291.1204
			3.0376			
	P(10)	3345.5211	2.9882	3291.9504	3.0368	3287.4328
			3.0410			
	P(11)	3341.5804	2.9917	3288.1848	3.0403	3283.6817
			3.0445			
	P(12)	3337.5714	2.9953	3284.3555	3.0438	3279.8672
			3.0480			
	P(13)	3333.4944	2.9990	3280.4624	3.0475	3275.9893
			3.0516			
	P(14)	3329.3494	3.0027	3276.5059	3.0511	3272.0483
			3.0553			
	P(15)	3325.1367	3.0065	3272.4859	3.0549	3268.0442
			3.0590			
	P(16)	3320.8563	3.0104	3268.4027	3.0587	3263.9772
			3.0629			

		$^{12}C^{16}O$		$^{13}C^{16}O$		$^{12}C^{18}O$	
v→v-2		1/λ	λ	1/λ	λ	1/λ	λ
20 - 18	P(9)	3299.4714	3.0299	3247.8558	3.0781	3243.4998	
			3.0822				
	P(10)	3295.6341	3.0334	3244.1869	3.0815	3239.8448	
			3.0857				
	P(11)	3291.7283	3.0370	3240.4541	3.0851	3236.1262	
			3.0892				
	P(12)	3287.7544	3.0407	3236.6575	3.0887	3232.3443	
			3.0928				
	P(13)	3283.7124	3.0444	3232.7972	3.0924	3228.4990	
			3.0965				
	P(14)	3279.6024	3.0483	3228.8734	3.0962	3224.5905	
			3.1003				
	P(15)	3275.4247	3.0521	3224.8862	3.1000	3220.6190	
			3.1041				
	P(16)	3271.1794	3.0561	3220.8358	3.1039	3216.5846	
			3.1080				
21 - 19	P(9)	3249.7176	3.0763	3200.2174	3.1239	3196.0362	
			3.1280				
	P(10)	3245.9152	3.0799	3196.5812	3.1274	3192.4137	
			3.1315				
	P(11)	3242.0445	3.0836	3192.8810	3.1311	3188.7276	
			3.1351				
	P(12)	3238.1055	3.0873	3189.1171	3.1347	3184.9781	
			3.1388				
	P(13)	3234.0985	3.0911	3185.2896	3.1385	3181.1654	
			3.1426				
	P(14)	3230.0235	3.0950	3181.3985	3.1424	3177.2894	
			3.1464				
	P(15)	3225.8808	3.0990	3177.4440	3.1463	3173.3505	
			3.1503				
	P(16)	3221.6705	3.1031	3173.4263	3.1502	3169.3486	
			3.1543				
22 - 20	P(9)	3200.1304	3.1240	3152.7355	3.1709	3148.7282	
			3.1750				
	P(10)	3196.3630	3.1276	3149.1319	3.1746	3145.1382	
			3.1786				
	P(11)	3192.5271	3.1314	3145.4645	3.1783	3141.4846	
			3.1823				

	P(12)	3188.6231	3.1352	3141.7332	3.1820	3137.7676
			3.1860			
	P(13)	3184.6511	3.1391	3137.9384	3.1859	3133.9874
			3.1899			
	P(14)	3180.6111	3.1431	3134.0800	3.1898	3130.1439
			3.1938			
	P(15)	3176.5033	3.1472	3130.1582	3.1938	3126.2375
			3.1978			
	P(16)	3172.3279	3.1513	3126.1732	3.1979	3122.2681
			3.2019			
2 3 - 21	P(9)	3150.7075	3.1730	3105.4083	3.2192	3101.5741
			3.2232			
	P(10)	3146.9750	3.1767	3101.8374	3.2230	3098.0166
			3.2269			
	P(11)	3143.1740	3.1806	3098.2025	3.2267	3094.3954
			3.2307			
	P(12)	3139.3049	3.1845	3094.5039	3.2306	3090.7109
			3.2346			
	P(13)	3135.3677	3.1885	3090.7417	3.2345	3086.9631
			3.2385			
	P(14)	3131.3626	3.1926	3086.9159	3.2385	3083.1521
			3.2425			
	P(15)	3127.2897	3.1967	3083.0268	3.2426	3079.2781
			3.2466			
	P(16)	3123.1492	3.2010	3079.0744	3.2468	3075.3412
			3.2507			
24 - 22	P(9)	3101.4458	3.2234	3058.2333	3.2689	3054.5715
			3.2728			
	P(10)	3097.7481	3.2272	3054.6950	3.2727	3051.0464
			3.2766			
	P(11)	3093.9820	3.2311	3051.0928	3.2766	3047.4577
			3.2805			
	P(12)	3090.1477	3.2351	3047.4267	3.2805	3043.8055
			3.2844			
	P(13)	3086.2454	3.2392	3043.6971	3.2845	3040.0901
			3.2884			
	P(14)	3082.2751	3.2434	3039.9039	3.2886	3036.3115
			3.2925			
	P(15)	3078.2370	3.2477	3036.0473	3.2928	3032.4699
			3.2967			
	P(16)	3074.1313	3.2520	3032.1275	3.2971	3028.5654
			3.3009			

		$^{12}C^{16}O$		$^{13}C^{16}O$		$^{12}C^{18}O$	
v→v-2		1/λ	λ	1/λ	λ	1/λ	λ
25 - 23	P(9)	3052.3415	3.2752	3011.2074	3.3200	3007.7173	
			3.3238				
	P(10)	3048.6785	3.2792	3007.7016	3.3238	3004.2245	
			3.3277				
	P(11)	3044.9472	3.2832	3004.1319	3.3278	3000.6681	
			3.3316				
	P(12)	3041.1477	3.2873	3000.4984	3.3318	2997.0484	
			3.3356				
	P(13)	3037.2801	3.2915	2996.8013	3.3359	2993.3653	
			3.3397				
	P(14)	3033.3446	3.2957	2993.0406	3.3401	2989.6190	
			3.3439				
	P(15)	3029.3412	3.3001	2989.2166	3.3444	2985.8097	
			3.3482				
	P(16)	3025.2702	3.3045	2985.3292	3.3487	2981.9375	
			3.3525				
26 - 24	P(9)	3003.3897	3.3286	2964.3266	3.3725	2961.0075	
			3.3762				
	P(10)	2999.7615	3.3326	2960.8533	3.3764	2957.5471	
			3.3802				
	P(11)	2996.0649	3.3367	2957.3161	3.3805	2954.0230	
			3.3842				
	P(12)	2992.3000	3.3409	2953.7151	3.3846	2950.4355	
			3.3883				
	P(13)	2988.4671	3.3452	2950.0504	3.3888	2946.7847	
			3.3925				
	P(14)	2984.5662	3.3496	2946.3222	3.3931	2943.0707	
			3.3968				
	P(15)	2980.5975	3.3541	2942.5305	3.3974	2939.2936	
			3.4012				
	P(16)	2976.5611	3.3586	2938.6756	3.4019	2935.4537	
			3.4056				
27 - 25	P(9)	2954.5848	3.3836	2917.5863	3.4265	2914.4377	
			3.4302				
	P(10)	2950.9913	3.3877	2914.1454	3.4305	2911.0095	
			3.4342				
	P(11)	2947.3293	3.3919	2910.6406	3.4347	2907.5177	
			3.4384				

	P(12)	2943.5991	3.3962	2907.0720	3.4389	2903.9624
			3.4426			
	P(13)	2939.8007	3.4006	2903.4397	3.4432	2900.3438
			3.4469			
	P(14)	2935.9344	3.4051	2899.7438	3.4476	2896.6619
			3.4512			
	P(15)	2932.0002	3.4096	2895.9845	3.4520	2892.9170
			3.4557			
	P(16)	2927.9983	3.4143	2892.1619	3.4566	2889.1092
			3.4603			
28 – 26	P(9)	2905.9203	3.4402	2870.9809	3.4821	2868.0023
			3.4857			
	P(10)	2902.3613	3.4445	2867.5724	3.4863	2864.6063
			3.4899			
	P(11)	2898.7339	3.4488	2864.1000	3.4905	2861.1467
			3.4941			
	P(12)	2895.0382	3.4532	2860.5637	3.4948	2857.6235
			3.4984			
	P(13)	2891.2743	3.4577	2856.9636	3.4992	2854.0370
			3.5028			
	P(14)	2887.4424	3.4623	2853.3000	3.5037	2850.3873
			3.5073			
	P(15)	2883.5426	3.4669	2849.5729	3.5083	2846.6744
			3.5118			
	P(16)	2879.5751	3.4717	2845.7825	3.5129	2842.8985
			3.5165			
29 – 27	P(9)	2857.3885	3.4987	2824.5041	3.5394	2821.6952
			3.5429			
	P(10)	2853.8640	3.5030	2821.1279	3.5436	2818.3313
			3.5472			
	P(11)	2850.2711	3.5074	2817.6877	3.5480	2814.9037
			3.5515			
	P(12)	2846.6098	3.5119	2814.1836	3.5524	2811.4126
			3.5559			
	P(13)	2842.8802	3.5165	2810.6158	3.5569	2807.8581
			3.5604			
	P(14)	2839.0826	3.5212	2806.9843	3.5615	2804.2403
			3.5650			
	P(15)	2835.2171	3.5260	2803.2894	3.5662	2800.5594
			3.5697			
	P(16)	2831.2837	3.5309	2799.5310	3.5710	2796.8154
			3.5745			

		$^{12}C^{16}O$		$^{13}C^{16}O$		$^{12}C^{18}O$	
v→v-2		1/λ	λ	1/λ	λ	1/λ	λ
30 - 28	P(9)	2808.9808	3.5590	2778.1485	3.5985	2775.5089	
			3.6019				
	P(10)	2805.4907	3.5634	2774.8046	3.6028	2772.1771	
			3.6062				
	P(11)	2801.9321	3.5679	2771.3966	3.6072	2768.7815	
			3.6106				
	P(12)	2798.3051	3.5725	2767.9246	3.6118	2765.3224	
			3.6152				
	P(13)	2794.6098	3.5773	2764.3888	3.6164	2761.7998	
			3.6198				
	P(14)	2790.8463	3.5821	2760.7894	3.6211	2758.2138	
			3.6245				
	P(15)	2787.0148	3.5870	2757.1264	3.6259	2754.5647	
			3.6293				
	P(16)	2783.1155	3.5920	2753.4000	3.6308	2750.8525	
			3.6342				
31 - 29	P(9)	2760.6873	3.6212	2731.9059	3.6594	2729.4355	
			3.6627				
	P(10)	2757.2316	3.6258	2728.5941	3.6638	2726.1357	
			3.6671				
	P(11)	2753.7072	3.6304	2725.2182	3.6684	2722.7720	
			3.6717				
	P(12)	2750.1143	3.6352	2721.7782	3.6730	2719.3447	
			3.6763				
	P(13)	2746.4531	3.6400	2718.2744	3.6777	2715.8539	
			3.6810				
	P(14)	2742.7236	3.6449	2714.7069	3.6826	2712.2997	
			3.6858				
	P(15)	2738.9260	3.6500	2711.0757	3.6875	2708.6822	
			3.6908				
	P(16)	2735.0605	3.6552	2707.3810	3.6925	2705.0016	
			3.6958				
32 - 30	P(9)	2712.4971	3.6856	2685.7669	3.7222	2683.4658	
			3.7254				
	P(10)	2709.0755	3.6902	2682.4872	3.7268	2680.1977	
			3.7300				
	P(11)	2705.5853	3.6950	2679.1432	3.7314	2676.8659	
			3.7346				

	P(12)	2702.0264	3.6998	2675.7352	3.7362	2673.4703
			3.7394			
	P(13)	2698.3990	3.7048	2672.2632	3.7411	2670.0111
			3.7442			
	P(14)	2694.7034	3.7099	2668.7274	3.7460	2666.4885
			3.7492			
	P(15)	2690.9395	3.7151	2665.1279	3.7511	2662.9025
			3.7542			
	P(16)	2687.1077	3.7204	2661.4648	3.7562	2659.2533
			3.7594			
33 - 31	P(9)	2664.3978	3.7521	2639.7212	3.7872	2637.5893
			3.7902			
	P(10)	2661.0103	3.7569	2636.4734	3.7918	2634.3531
			3.7949			
	P(11)	2657.5540	3.7618	2633.1613	3.7966	2631.0529
			3.7997			
	P(12)	2654.0290	3.7668	2629.7850	3.8015	2627.6889
			3.8045			
	P(13)	2650.4354	3.7719	2626.3447	3.8065	2624.2612
			3.8095			
	P(14)	2646.7733	3.7771	2622.8405	3.8115	2620.7700
			3.8146			
	P(15)	2643.0430	3.7824	2619.2724	3.8167	2617.2154
			3.8197			
	P(16)	2639.2445	3.7879	2615.6408	3.8220	2613.5974
			3.8250			
34 - 32	P(9)	2616.3758	3.8210	2593.7571	3.8543	2591.7948
			3.8572			
	P(10)	2613.0223	3.8259	2590.5412	3.8591	2588.5903
			3.8620			
	P(11)	2609.5998	3.8309	2587.2608	3.8640	2585.3216
			3.8669			
	P(12)	2606.1084	3.8360	2583.9161	3.8690	2581.9891
			3.8719			
	P(13)	2602.5483	3.8413	2580.5073	3.8741	2578.5928
			3.8770			
	P(14)	2598.9197	3.8466	2577.0345	3.8793	2575.1328
			3.8822			
	P(15)	2595.2226	3.8521	2573.4978	3.8846	2571.6092
			3.8875			
	P(16)	2591.4573	3.8577	2569.8973	3.8901	2568.0223
			3.8929			

		$^{12}C^{16}O$		$^{13}C^{16}O$		$^{12}C^{18}O$	
v→v-2		1/λ	λ	1/λ	λ	1/λ	λ
35 - 33	P(9)	2568.4160	3.8923	2547.8619	3.9237	2546.0697	
			3.9265				
	P(10)	2565.0963	3.8974	2544.6777	3.9286	2542.8966	
			3.9314				
	P(11)	2561.7074	3.9025	2541.4289	3.9336	2539.6594	
			3.9364				
	P(12)	2558.2496	3.9078	2538.1157	3.9388	2536.3582	
			3.9415				
	P(13)	2554.7228	3.9132	2534.7382	3.9440	2532.9930	
			3.9467				
	P(14)	2551.1274	3.9187	2531.2966	3.9494	2529.5641	
			3.9521				
	P(15)	2547.4633	3.9243	2527.7909	3.9549	2526.0715	
			3.9576				
	P(16)	2543.7308	3.9301	2524.2214	3.9605	2522.5153	
			3.9631				
36 - 34	P(9)	2520.5019	3.9663	2502.0214	3.9956	2500.3999	
			3.9982				
	P(10)	2517.2158	3.9715	2498.8688	4.0006	2497.2583	
			4.0032				
	P(11)	2513.8604	3.9768	2495.6514	4.0058	2494.0523	
			4.0084				
	P(12)	2510.4358	3.9822	2492.3695	4.0111	2490.7822	
			4.0136				
	P(13)	2506.9422	3.9878	2489.0232	4.0165	2487.4481	
			4.0190				
	P(14)	2503.3796	3.9934	2485.6126	4.0220	2484.0499	
			4.0245				
	P(15)	2499.7483	3.9992	2482.1378	4.0276	2480.5880	
			4.0301				
	P(16)	2496.0484	4.0052	2478.5989	4.0334	2477.0624	
			4.0359				
37 - 35	P(9)	2472.6151	4.0431	2456.2202	4.0701	2454.7702	
			4.0725				
	P(10)	2469.3625	4.0484	2453.0990	4.0753	2451.6599	
			4.0777				
	P(11)	2466.0404	4.0539	2449.9130	4.0806	2448.4851	
			4.0830				

	P(12)	2462.6488	4.0595	2446.6622	4.0860	2445.2459
			4.0884			
	P(13)	2459.1881	4.0652	2443.3468	4.0916	2441.9425
			4.0939			
	P(14)	2455.6582	4.0710	2439.9669	4.0972	2438.5750
			4.0996			
	P(15)	2452.0593	4.0770	2436.5227	4.1030	2435.1436
			4.1053			
	P(16)	2448.3916	4.0831	2433.0143	4.1089	2431.6482
			4.1112			
38 - 36	P(9)	2424.7357	4.1230	2410.4413	4.1474	2409.1639
			4.1496			
	P(10)	2421.5164	4.1284	2407.3514	4.1527	2406.0847
			4.1549			
	P(11)	2418.2273	4.1341	2404.1964	4.1582	2402.9409
			4.1604			
	P(12)	2414.8686	4.1398	2400.9766	4.1638	2399.7325
			4.1659			
	P(13)	2411.4405	4.1457	2397.6919	4.1695	2396.4596
			4.1716			
	P(14)	2407.9429	4.1517	2394.3426	4.1753	2393.1225
			4.1774			
	P(15)	2404.3762	4.1579	2390.9287	4.1813	2389.7212
			4.1834			
	P(16)	2400.7403	4.1642	2387.4504	4.1873	2386.2559
			4.1894			
39 - 37	P(9)	2376.8418	4.2060	2364.6660	4.2277	2363.5627
			4.2297			
	P(10)	2373.6556	4.2117	2361.6073	4.2332	2360.5145
			4.2351			
	P(11)	2370.3994	4.2175	2358.4833	4.2388	2357.4014
			4.2407			
	P(12)	2367.0733	4.2234	2355.2941	4.2445	2354.2235
			4.2464			
	P(13)	2363.6774	4.2295	2352.0399	4.2504	2350.9811
			4.2523			
	P(14)	2360.2119	4.2357	2348.7209	4.2564	2347.6741
			4.2583			
	P(15)	2356.6769	4.2420	2345.3370	4.2625	2344.3027
			4.2644			
	P(16)	2353.0726	4.2485	2341.8885	4.2688	2340.8670
			4.2707			

APPENDIX IV. Reflective diffraction grating for tunable FO CO laser

One more perspective method to provide the complete discrimination between lasing in overtone and fundamental bands is based on using a reflective diffraction grating as a mirror of the laser cavity. It is assumed that this grating operates in autocollimating mode (Littrov configuration). This grating should withstand high radiation doses, which is possible only, if it is mechanically ruled. It should have low losses as for absorption by the surface material, as for reflection in all higher diffraction orders. To avoid absorption it is necessary to coat the ground material (i.e. super-invar) with high-reflecting metal-dielectric composition. To concentrate the reflected radiation into a sole diffraction order, the grooves should be of a special profile.

During recent years, the technology of mechanically ruled blazed infrared reflective gratings has made a considerable progress and reflection efficiencies of close to 99% have been achieved. It is essential to have a ruling density so that only the first order reflection is possible for the wavelength in question since the existence of the second order diffraction automatically means further losses.

We have information about two specimens of the gratings of this sort. The first was manufactured by Hyperfine Inc., Boulder, the second by Ziess Oberkochen, Germany. Both samples had a high uniform reflectance in the first diffraction order (~ 99%) in a board spectral range from 2.75 up to 4.0 μm. By simultaneous varying of the groove profile and ruling density, the ratio of fractions reflected in the first and zeroth orders as a function of the frequency in the laser spectrum can be controlled.

With a help of such a grating, the selective cavity for the FO CO laser may be arranged in two ways. The first is when the diffraction grating with high spectral-uniform reflectivity serves as a rear mirror with low losses and an output mirror is a dielectric one with a broad-band transmittance of 6-8% for our conditions. The second way is when the zeroth diffraction-order reflection serves for outcoupling of laser beam also about 6-8% of the incident to the grating laser intensity.